Chin. Ann. Math.
36B(5), 2015, 659–688
DOI: 10.1007/s11401-015-0930-8

Chinese Annals of Mathematics, Series B

A Penalty-Regularization-Operator Splitting Method for the Numerical Solution of a Scalar Eikonal Equation*

Alexandre CABOUSSAT[1] Roland GLOWINSKI[2]

(*In Honor of the Scientific Contributions of Professor Luc Tartar*)

Abstract In this article, we discuss a numerical method for the computation of the minimal and maximal solutions of a steady scalar Eikonal equation. This method relies on a penalty treatment of the nonlinearity, a biharmonic regularization of the resulting variational problem, and the time discretization by operator-splitting of an initial value problem associated with the Euler-Lagrange equations of the regularized variational problem. A low-order finite element discretization is advocated since it is well-suited to the low regularity of the solutions. Numerical experiments show that the method sketched above can capture efficiently the extremal solutions of various two-dimensional test problems and that it has also the ability of handling easily domains with curved boundaries.

Keywords Eikonal equation, Minimal and maximal solutions, Regularization methods, Penalization of equality constraints, Dynamical flow, Operator splitting, Finite element methods
2000 MR Subject Classification 65N30, 65K10, 65M60, 49M20, 35F30

1 Introduction

Various mathematical models in science and engineering lead to the prototypical Eikonal equation $|\nabla u| = 1$; this is the case particularly in optics, wave propagation, material science, differential geometry (geodesics) (see [32]), geophysics (see [37]), and image processing. The analysis of such nonlinear models can be found in [14] (see also the references therein). Actually, the Eikonal equation is often associated with the Hamilton-Jacobi equation for wave propagation (as shown in [40]).

In this article, we are interested in the computation of the approximate solutions of the Dirichlet problem for a steady Eikonal equation. Namely, we want to find $u : \Omega \subset \mathbb{R}^2 \to \mathbb{R}$ satisfying

$$\begin{cases} |\nabla u| = 1 & \text{in } \Omega, \\ u = g & \text{on } \partial\Omega, \end{cases} \tag{1.1}$$

Manuscript received May 2, 2014. Revised August 8, 2014.
[1]Haute Ecole de Gestion de Genève, HES-SO//University of Applied Sciences, Western Switzerland, Route de Drize 7, 1227 Carouge, Switzerland. E-mail: alexandre.caboussat@hesge.ch
[2]Department of Mathematics, University of Houston, 4800 Calhoun Rd, Houston, Texas 77204-3008, USA. E-mail: roland@math.uh.edu
*This work was supported by the National Science Foundation (No. DMS-0913982).

where g is a given data, and $|\cdot|$ is the canonical Euclidean norm. Problem (1.1) is a Dirichlet problem for the scalar Eikonal equation. Vector Eikonal equations, which are natural generalizations of (1.1), have been discussed in [15–17] for origami modeling. All these problems are examples of implicitly nonlinear equations (see [8, 22]).

Numerical methods for the solution of this type of implicitly nonlinear equations can be found in, e.g., [5, 12–13, 27]. Related methods can be used for the solutions of the Hamilton-Jacobi equations and of some obstacle problems. Among these numerical methods, let us mention the fast marching methods (see [40]), the fast sweeping methods (see [42]), and the level-set-based methods (see [2]). Among the computational issues which have been and are currently investigated, let us mention the computational cost, the influence of the space discretization mesh, and the design of fast algorithms (see related references [30–31, 37, 41]). Similar problems, involving the infinity-Laplacian operator, arise in sand mechanics (see, e.g., [1, 3, 35–36]).

Due to the low regularity and the possible multiplicity of the solutions of the scalar Eikonal equation, these solutions have to be defined in a generalized sense, the most commonly accepted one being the notion of viscosity solutions (see, e.g., [11]). Other approaches are available as shown in, e.g., [29].

Most methods for the numerical solution of the scalar Eikonal equation view it as a nonlinear hyperbolic problem. In this article, we take a different point of view, and attempt to solve (1.1) by using a calculus of variations approach relying on elliptic solvers and on the time-discretization by operator-splitting of an initial value problem associated with an Euler-Lagrange equation. Our approach, which is also well-suited to the solution of some Eikonal systems (see [12–13]), focuses on the computation of minimal and maximal solutions of (1.1), using a methodology combining: (i) A quadratic penalization of the Ginzburg-Landau type to relax the equation $|\nabla u| = 1$, considered as a nonlinear equality constraint. (ii) A linear or nonlinear biharmonic regularization (see [3, 21, 28]). (iii) The use of an operator-splitting scheme à la Marchuk-Yanenko to time-discretize an initial value problem associated with the Euler-Lagrange equation of the above regularized problem. (iv) A low-order C^0-conforming finite element approximation, well-suited to the Lipschitz continuous regularity of the solutions and to domains with a curved boundary.

The operator-splitting approach allows the decoupling of the differential operators from the Ginzburg-Landau nonlinearity. Actually, these techniques have been successfully applied by the authors to other situations, such as Monge-Ampère and Pucci equations (see [6, 9, 18–19, 26]), visco-plastic or particulate flow (see [20, 24]) and other problems involving non-smooth operators (see [3–4, 33]).

The article is organized as follows: In Section 2, we formulate particular cases of (1.1), leading to minimal and maximal solutions. Equivalent and regularized formulations are given in Section 3. Our computational approach is described in Section 4, while in Section 5 we briefly describe another regularization approach. The finite element implementation of our methodology is discussed in Section 6 with the corresponding numerical results being presented in Section 7. Finally, among other comments, a viscosity interpretation of our methodology will be given in Section 8.

2 Problem Formulation

Let Ω be a bounded domain of $\mathbb{R}^2$; we suppose that the boundary $\Gamma := \partial\Omega$ is at least Lipschitz continuous in the sense of Nečas [34]. The steady scalar Eikonal equation we want to solve reads as follows: Find $u : \Omega \to \mathbb{R}$ verifying

$$\begin{cases} |\nabla u| = 1 & \text{in } \Omega, \\ u = g & \text{on } \Gamma. \end{cases} \tag{2.1}$$

We observe that, up to the addition of a constant, we can always suppose that $g \geq 0$. Since problem (2.1) has infinitely many solutions, in general, it makes sense to enforce uniqueness by imposing additional conditions. In this article, we will impose on the solution to be maximal in the sense of $L^1(\Omega)$ (actually, we can also impose on the solution to be minimal).

Remark 2.1 If the equation $|\nabla u| = 1$ is replaced by the more general situation $|\nabla u| = f(\geq 0)$, the numerical approach presented in this work also applies with straightforward modifications.

In order to obtain the maximal solution, we actually require u to maximize the linear functional

$$v \to \int_\Omega v \mathrm{d}\mathbf{x} \tag{2.2}$$

over

$$E_g = \{v \in H^1(\Omega),\ v = g \text{ on } \Gamma, |\nabla v| = 1 \text{ in } \Omega\}, \tag{2.3}$$

instead of maximizing the L^1-norm over E_g. This change of the cost function is easy to justify: Indeed suppose that u maximizes the functional (2.2) over E_g. Since $g \geq 0$ and $|\nabla |u|| = |\nabla u|$, we also have $|u| \in E_g$. By the definition of u, we have

$$\int_\Omega |u| \, \mathrm{d}\mathbf{x} \leq \int_\Omega u \mathrm{d}\mathbf{x}.$$

On the other hand, the relation $u \leq |u|$ implies that

$$\int_\Omega u \mathrm{d}\mathbf{x} \leq \int_\Omega |u| \, \mathrm{d}\mathbf{x}.$$

It follows that

$$\int_\Omega [|u| - u] \, \mathrm{d}\mathbf{x} = 0.$$

The non-negativity of the integrand $|u| - u \geq 0$ implies that $u = |u|$, that is, the non-negativity of u. Actually, we can easily prove that the above function is also the upper hull of all the functions in E_g, that is, the (necessarily unique (see [38])) function u of E_g verifying

$$u(\mathbf{x}) \geq v(\mathbf{x}), \quad \forall v \in E_g,\ \forall \mathbf{x} \in \Omega. \tag{2.4}$$

Remark 2.2 In order to find the smallest solution of (2.1) in the sense of (2.4), that is,

$$u(\mathbf{x}) \leq v(\mathbf{x}), \quad \forall v \in E_g,\ \forall \mathbf{x} \in \Omega, \tag{2.5}$$

we would minimize over E_g the functional

$$v \rightarrow \int_\Omega v \mathrm{d}\mathbf{x}.$$

Remark 2.3 If $g = 0$, the maximizer of (2.2) is nothing but the distance function to the boundary of the domain $\mathbf{x} \rightarrow \delta(\mathbf{x}, \Gamma)$. For example, in one dimension of space, if $\Omega = (0,1)$, then $u(x) = \min(x, 1-x)$; in two dimensions of space, if $\Omega = (0,1) \times (0,1)$, then

$$u(\mathbf{x}) = u(x_1, x_2) = \min(x_1, x_2, 1-x_1, 1-x_2), \quad \forall \mathbf{x} = \{x_1, x_2\} \in \Omega.$$

If Ω is the disk of radius R centered at 0, then $u(\mathbf{x}) = u(x_1, x_2) = R - \sqrt{x_1^2 + x_2^2}$.

In the remainder of this article, we describe a numerical method for the approximate computation of the maximal and minimal solutions in the general case.

3 Modeling, Regularization and Penalization

Let $C > 0$ be a given positive constant. We first note that there is an equivalence between

$$u = \arg\max_{v \in E_g} \int_\Omega v \mathrm{d}\mathbf{x} \tag{3.1}$$

and

$$u = \arg\min_{v \in E_g} \Big[\frac{1}{2}\int_\Omega |\nabla v|^2 \mathrm{d}\mathbf{x} - C\int_\Omega v \mathrm{d}\mathbf{x}\Big]. \tag{3.2}$$

The main difficulty with (3.2) is the nonlinear constraint $|\nabla v| = 1$ (which is equivalent to $|\nabla v|^2 = 1$). To handle this constraint we are going to use a penalization approach preserving the differentiability of the cost functional. Let $\varepsilon > 0$ be a small parameter; we thus approximate (3.2) by

$$u_\varepsilon = \arg\min_{v \in W_g^{1,4}} \Big[\frac{1}{2}\int_\Omega |\nabla v|^2 \mathrm{d}\mathbf{x} - C\int_\Omega v \mathrm{d}\mathbf{x} + \frac{1}{4\varepsilon}\int_\Omega (|\nabla v|^2 - 1)^2 \mathrm{d}\mathbf{x}\Big], \tag{3.3}$$

where

$$W_g^{1,4} = \left\{v \in W^{1,4}(\Omega)\,,\, v = g \text{ on } \Gamma\right\}. \tag{3.4}$$

Based on past experience with related problems (see, e.g., [6, 12–13]), we introduce a biharmonic regularization. We thus consider a positive constant $\eta > 0$ and a regularized variant of (3.3) that reads:

$$\begin{aligned} u_\varepsilon^\eta = \arg & \min_{v \in W_g^{1,4} \cap H^2(\Omega)} \Big[\frac{\eta}{2}\int_\Omega \left|\nabla^2 v\right|^2 \mathrm{d}\mathbf{x} + \frac{1}{2}\int_\Omega |\nabla v|^2 \mathrm{d}\mathbf{x} \\ & - C\int_\Omega v \mathrm{d}\mathbf{x} + \frac{1}{4\varepsilon}\int_\Omega (|\nabla v|^2 - 1)^2 \mathrm{d}\mathbf{x}\Big]. \end{aligned} \tag{3.5}$$

The introduction of the regularization term $\frac{\eta}{2}\int_\Omega \left|\nabla^2 v\right|^2 \mathrm{d}\mathbf{x}$ corresponds to adding the biharmonic term $-\eta\nabla^2 u$ to the first-order optimality conditions, together with the natural boundary condition $\nabla^2 u = 0$ on Γ.

Remark 3.1 (A Nonlinear Biharmonic Regularization) Another regularized variant of (3.3) that is inspired from image-processing techniques (see [10]) reads as follows:

$$\begin{aligned} u_\varepsilon^\eta = \arg \min_{v \in W_g^{1,4} \cap W^{2,1}(\Omega)} \Big[& \eta \int_\Omega \sqrt{1 + |\nabla^2 v|^2} \mathrm{d}\mathbf{x} + \frac{1}{2} \int_\Omega |\nabla v|^2 \, \mathrm{d}\mathbf{x} \\ & - C \int_\Omega v \mathrm{d}\mathbf{x} + \frac{1}{4\varepsilon} \int_\Omega (|\nabla v|^2 - 1)^2 \mathrm{d}\mathbf{x} \Big]. \end{aligned} \tag{3.6}$$

In the following sections, we are going to discuss mainly the iterative solution of problem (3.5). Due to the interesting features of problem (3.6), we will discuss it briefly aside in Section 5.

Remark 3.2 In order to capture the minimal solution instead of the maximal solution, it suffices to change C in $-C$ in (3.2) (and in (3.5)–(3.6)), C still being a strictly positive constant.

Remark 3.3 For the sake of rigor, we should replace in (3.5), g by a regularized version $g_\eta \in H^{\frac{3}{2}}(\Gamma)$, such that $\lim\limits_{\eta \to 0} g_\eta = g$. Actually, the numerical results reported in Section 7 show that using Lipschitz continuous functions g without the $H^{\frac{3}{2}}(\Gamma)$-regularity has no computational incidence in practice.

4 On the Solution of the Regularized Variational Problem

4.1 Mixed formulation and optimality conditions

After dropping the indices ε and η, (3.5) reads as follows:

$$\begin{aligned} u = \arg \min_{v \in W_g^{1,4} \cap H^2(\Omega)} \Big[& \frac{\eta}{2} \int_\Omega \left|\nabla^2 v\right|^2 \mathrm{d}\mathbf{x} + \frac{1}{2} \int_\Omega |\nabla v|^2 \, \mathrm{d}\mathbf{x} \\ & - C \int_\Omega v \mathrm{d}\mathbf{x} + \frac{1}{4\varepsilon} \int_\Omega (|\nabla v|^2 - 1)^2 \mathrm{d}\mathbf{x} \Big]. \end{aligned} \tag{4.1}$$

In order to solve (4.1), let us define the function u_1 as the unique solution of the following linear variational problem: Find $u_1 \in H_g^1 := \left\{ v \in H^1(\Omega) \, , \, v = g \text{ on } \Gamma \right\}$ satisfying

$$\int_\Omega \nabla u_1 \cdot \nabla v \mathrm{d}\mathbf{x} = \int_\Omega v \mathrm{d}\mathbf{x}, \quad \forall v \in H_0^1(\Omega). \tag{4.2}$$

The function u_1 is the solution of the Poisson-Dirichlet problem: $-\nabla^2 u_1 = 1$ in Ω, with boundary conditions $u = g$ on Γ. If Γ is smooth and/or Ω convex, the function u_1 has enough regularity to belong to $W_g^{1,4}(\Omega)$. Since $W_g^{1,4}(\Omega) \subset H_g^1(\Omega)$, it follows from (4.2) that

$$\int_\Omega \nabla u_1 \cdot \nabla (v - u_1) \mathrm{d}\mathbf{x} = \int_\Omega (v - u_1) \mathrm{d}\mathbf{x}, \quad \forall v \in W_g^{1,4}(\Omega). \tag{4.3}$$

Relationship (4.3) implies that $\int_\Omega v \mathrm{d}\mathbf{x} = \int_\Omega u_1 \mathrm{d}\mathbf{x} - \int_\Omega |\nabla u_1|^2 \, \mathrm{d}\mathbf{x} + \int_\Omega \nabla u_1 \cdot \nabla v \mathrm{d}\mathbf{x}$ for all $v \in W_g^{1,4}(\Omega)$, which implies in turn that (4.1) is equivalent to

$$\begin{aligned} u = \arg \min_{v \in W_g^{1,4} \cap H^2(\Omega)} \Big[& \frac{\eta}{2} \int_\Omega \left|\nabla^2 v\right|^2 \mathrm{d}\mathbf{x} + \frac{1}{2} \int_\Omega |\nabla v|^2 \, \mathrm{d}\mathbf{x} \\ & - C \int_\Omega \nabla u_1 \cdot \nabla v \mathrm{d}\mathbf{x} + \frac{1}{4\varepsilon} \int_\Omega (|\nabla v|^2 - 1)^2 \mathrm{d}\mathbf{x} \Big]. \end{aligned} \tag{4.4}$$

The rationale behind the introduction of u_1 and the alternative formulation (4.4) is to have ∇u, instead of u, as the master unknown, the new problem having better decomposition properties. We denote by $\mathbf{p}$ the vector-valued function ∇u, and define the vector space $\mathbf{Q}$ by

$$\mathbf{Q} = \{\mathbf{q} \in L^4(\Omega)^2\,,\ \nabla \cdot \mathbf{q} \in L^2(\Omega)\}. \tag{4.5}$$

Setting $\mathbf{q} := \nabla v$, there is equivalence between (4.4) and the following non-convex nonlinear variational problem (of the mixed type):

$$\begin{aligned} \mathbf{p} = \arg\min_{\mathbf{q}\in\mathbf{Q}} \Big[& \frac{\eta}{2}\int_\Omega |\nabla \cdot \mathbf{q}|^2\, \mathrm{d}\mathbf{x} + \frac{1}{2}\int_\Omega |\mathbf{q}|^2\, \mathrm{d}\mathbf{x} \\ & - C\int_\Omega \nabla u_1 \cdot \mathbf{q}\mathrm{d}\mathbf{x} + \frac{1}{4\varepsilon}\int_\Omega (|\mathbf{q}|^2 - 1)^2 \mathrm{d}\mathbf{x} + I_\nabla(\mathbf{q})\Big], \end{aligned} \tag{4.6}$$

where $I_\nabla(\cdot)$ is the indicator functional of the space $\nabla W_g^{1,4}(\Omega)$, that is,

$$I_\nabla(\mathbf{q}) = \begin{cases} 0, & \text{if } \mathbf{q} \in \nabla W_g^{1,4}(\Omega), \\ +\infty, & \text{if } \mathbf{q} \in \mathbf{Q}\backslash\nabla W_g^{1,4}(\Omega). \end{cases} \tag{4.7}$$

We observe that in (4.6), the quartic term is of the Ginzburg-Landau type. In the variational form, the Euler-Lagrange equation associated with (4.6) reads as follows: Find $\mathbf{p} \in \mathbf{Q}$ satisfying

$$\begin{aligned} & \eta\int_\Omega (\nabla\cdot\mathbf{p})(\nabla\cdot\mathbf{q})\mathrm{d}\mathbf{x} + \int_\Omega \mathbf{p}\cdot\mathbf{q}\mathrm{d}\mathbf{x} - C\int_\Omega \nabla u_1\cdot\mathbf{q}\mathrm{d}\mathbf{x} \\ & + \frac{1}{\varepsilon}\int_\Omega (|\mathbf{p}|^2 - 1)\mathbf{p}\cdot\mathbf{q}\mathrm{d}\mathbf{x} + \langle \partial I_\nabla(\mathbf{p}), \mathbf{q}\rangle = 0, \quad \forall \mathbf{q}\in\mathbf{Q}. \end{aligned} \tag{4.8}$$

Here $\partial I_\nabla(\mathbf{p})$ denotes the subgradient of the functional $I_\nabla(\cdot)$ evaluated at $\mathbf{p}$ (see [38]).

Remark 4.1 Instead of defining u_1 as the solution of $-\nabla^2 u_1 = 1$ in Ω, together with $u_1 = g$ on Γ, we could have defined it as the solution of $-\nabla^2 u_1 = 1$ in Ω, together with $u_1 = 0$ on Γ.

4.2 Initial-value problem and operator-splitting

We associate with (4.8) the following initial-value problem (flow in the dynamical system terminology): Find $\mathbf{p}(t) \in \mathbf{Q}$ for a.e. $t \in (0, +\infty)$ satisfying

$$\begin{cases} \displaystyle\int_\Omega \frac{\partial \mathbf{p}}{\partial t}\cdot\mathbf{q}\mathrm{d}\mathbf{x} + \eta\int_\Omega (\nabla\cdot\mathbf{p})(\nabla\cdot\mathbf{q})\mathrm{d}\mathbf{x} + \int_\Omega \mathbf{p}\cdot\mathbf{q}\mathrm{d}\mathbf{x} - C\int_\Omega \nabla u_1\cdot\mathbf{q}\mathrm{d}\mathbf{x} \\ \displaystyle\quad + \frac{1}{\varepsilon}\int_\Omega (|\mathbf{p}|^2 - 1)\mathbf{p}\cdot\mathbf{q}\mathrm{d}\mathbf{x} + \langle \partial I_\nabla(\mathbf{p}), \mathbf{q}\rangle = 0, \quad \forall \mathbf{q}\in\mathbf{Q}, \\ \mathbf{p}(0) = \mathbf{p}_0. \end{cases} \tag{4.9}$$

Our aim is to find a stationary solution to the initial-value problem (IVP for short) (4.9). In order to solve this IVP, we advocate an operator-splitting scheme à la Marchuk-Yanenko (see, e.g., [24, Chapter 6]) for its robustness and simplicity. Note that other schemes are available (like the Strang symmetrized one). Let us denote by $\tau > 0$ a time-discretization step and set $t^n = n\tau,\ n = 0, 1, 2, \cdots$. Let $\mathbf{p}^n$ be an approximation of $\mathbf{p}(t^n)$. In order to solve (4.9), we advocate the following operator-splitting scheme: Initialize with

$$\mathbf{p}^0 = \mathbf{p}_0. \tag{4.10}$$

For $n \geq 0$, $\mathbf{p}^n$ being known, we compute $\mathbf{p}^{n+\frac{1}{2}}$ and $\mathbf{p}^{n+1}$ successively via the solution of:

$$\begin{cases} \mathbf{p}^{n+\frac{1}{2}} \in \mathbf{Q}, \\ \displaystyle\int_\Omega \frac{\mathbf{p}^{n+\frac{1}{2}} - \mathbf{p}^n}{\tau} \cdot \mathbf{q} d\mathbf{x} + \frac{1}{\varepsilon} \int_\Omega \left(\left| \mathbf{p}^{n+\frac{1}{2}} \right|^2 - 1 \right) \mathbf{p}^{n+\frac{1}{2}} \cdot \mathbf{q} d\mathbf{x} = 0, \\ \forall \mathbf{q} \in \mathbf{Q}, \end{cases} \tag{4.11}$$

$$\begin{cases} \mathbf{p}^{n+1} \in \mathbf{Q}, \\ \displaystyle\int_\Omega \frac{\mathbf{p}^{n+1} - \mathbf{p}^{n+\frac{1}{2}}}{\tau} \cdot \mathbf{q} d\mathbf{x} + \eta \int_\Omega (\nabla \cdot \mathbf{p}^{n+1})(\nabla \cdot \mathbf{q}) d\mathbf{x} + \int_\Omega \mathbf{p}^{n+1} \cdot \mathbf{q} d\mathbf{x} \\ \displaystyle -C \int_\Omega \nabla u_1 \cdot \mathbf{q} d\mathbf{x} + \left\langle \partial I_\nabla (\mathbf{p}^{n+1}), \mathbf{q} \right\rangle = 0, \quad \forall \mathbf{q} \in \mathbf{Q}. \end{cases} \tag{4.12}$$

Actually, problem (4.11) can be solved point-wise, corresponding thus to an infinite family of low-dimensional optimization problems. On the other hand, (4.12) is a classical linear variational problem written in a mixed form. We are going to discuss in the following sections the solution of these two problems. The initialization of algorithm (4.10)–(4.12) is the topic of the next remark.

Remark 4.2 (Initialization of the IVP) Choosing sensibly $\mathbf{p}^0$ in (4.10) is an important issue in order to reduce the number of time steps necessary to achieve convergence. We thus advocate the following approach: Solve $-\nabla^2 u_0 = C/|C|$ in Ω, with $u_0 = g$ on Γ. Then, we define $\mathbf{p}^0$ by

$$\mathbf{p}^0(\mathbf{x}) = \begin{cases} \dfrac{\nabla u_0(\mathbf{x})}{|\nabla u_0(\mathbf{x})|}, & \text{if } \nabla u_0(\mathbf{x}) \neq \mathbf{0}, \\ \mathbf{0}, & \text{otherwise.} \end{cases}$$

4.3 Solution of the local optimization problems

Problem (4.11) does not involve any derivatives. Thus it can be solved locally for almost every point $\mathbf{x} \in \Omega$. Rewriting (4.11) locally, we see that $\mathbf{p}^{n+\frac{1}{2}}(\mathbf{x})$ verifies

$$\mathbf{p}^{n+\frac{1}{2}}(\mathbf{x}) \Big[\Big(1 - \frac{\tau}{\varepsilon} \Big) + \frac{\tau}{\varepsilon} |\mathbf{p}^{n+\frac{1}{2}}(\mathbf{x})|^2 \Big] = \mathbf{p}^n(\mathbf{x}), \quad \text{a.e. } \mathbf{x} \text{ on } \Omega. \tag{4.13}$$

Taking the canonical Euclidean norm of both sides of the vector-valued equation (4.13), it follows that $|\mathbf{p}^{n+\frac{1}{2}}(\mathbf{x})|$ is a solution of the real-valued cubic equation:

$$\frac{\tau}{\varepsilon} z^3 + \left(1 - \frac{\tau}{\varepsilon} \right) z = |\mathbf{p}^n(\mathbf{x})| \,. \tag{4.14}$$

If the condition $\tau \leq \varepsilon$ holds, the equation (4.14) has a unique solution, necessarily non-negative. Once $|\mathbf{p}^{n+\frac{1}{2}}(\mathbf{x})|$ is known, we obtain $\mathbf{p}^{n+\frac{1}{2}}(\mathbf{x})$ from (4.13) by setting

$$\mathbf{p}^{n+\frac{1}{2}}(\mathbf{x}) = \Big(\frac{1}{\left(1 - \frac{\tau}{\varepsilon} \right) + \frac{\tau}{\varepsilon} |\mathbf{p}^{n+\frac{1}{2}}(\mathbf{x})|^2} \Big) \mathbf{p}^n(\mathbf{x}). \tag{4.15}$$

To solve the nonlinear equation (4.14), we advocate the Newton-Raphson method starting from the initial guess $z^0 = 1$; the consecutive iterates are thus, for $k \geq 0$,

$$z^{k+1} = z^k - \frac{\frac{\tau}{\varepsilon} (z^k)^3 + \left(1 - \frac{\tau}{\varepsilon} \right) z^k - |\mathbf{p}^n(\mathbf{x})|}{3 \left(\frac{\tau}{\varepsilon} \right) z^2 + \left(1 - \frac{\tau}{\varepsilon} \right)}. \tag{4.16}$$

In practice, after an appropriate finite difference or finite element approximation, we have to solve at each time step a cubic equation such as (4.14) for each point (resp. triangle) of the associated finite difference (resp. finite element) grid. Since Ω is bounded in $\mathbb{R}^2$, the number of such cubic equations is of the order of h^{-2}, where h is a space-discretization step.

4.4 Solution of the linear variational problems

Problem (4.12) is simpler to solve than it looks like. Indeed, setting

$$\nabla u^{n+1} := \mathbf{p}^{n+1},$$

problem (4.12) is equivalent to finding $u^{n+1} \in H^2(\Omega) \cap H^1_g(\Omega)$ that satisfy

$$\begin{aligned}&\int_\Omega \frac{\nabla u^{n+1} - \mathbf{p}^{n+\frac{1}{2}}}{\tau} \cdot \nabla v \mathrm{d}\mathbf{x} + \eta \int_\Omega (\nabla^2 u^{n+1})(\nabla^2 v)\mathrm{d}\mathbf{x} \\ &+ \int_\Omega \nabla u^{n+1} \cdot \nabla v \mathrm{d}\mathbf{x} - C\int_\Omega v \mathrm{d}\mathbf{x} = 0, \quad \forall v \in H^2(\Omega) \cap H^1_0(\Omega).\end{aligned} \tag{4.17}$$

Problem (4.17) is nothing but a variational formulation of the following biharmonic problem:

$$\begin{cases} -(1+\tau)\nabla^2 u^{n+1} + \eta\tau\nabla^4 u^{n+1} = \tau C - \nabla \cdot \mathbf{p}^{n+\frac{1}{2}} \quad \text{in } \Omega, \\ u^{n+1} = g \ \text{ on } \ \Gamma, \quad \nabla^2 u^{n+1} = 0 \quad \text{on } \ \Gamma. \end{cases}$$

Such a biharmonic problem is equivalent to the following system of two well-posed second-order linear elliptic problems:

$$\begin{cases} (1+\tau) w^{n+1} - \eta\tau\nabla^2 w^{n+1} = \tau C - \nabla \cdot \mathbf{p}^{n+\frac{1}{2}} \quad \text{in } \Omega, \\ w^{n+1} = 0 \quad \text{on } \ \Gamma, \end{cases}$$

$$\begin{cases} -\nabla^2 u^{n+1} = w^{n+1} \quad \text{in } \Omega, \\ u^{n+1} = g \quad \text{on } \ \Gamma. \end{cases}$$

Anticipating Section 6, boundary-layer considerations suggest taking $\eta\tau \simeq h^2$ with h being a space-discretization step. Many direct and iterative methods are available for the numerical solution of the above two elliptic boundary value problems (in fact, of their discrete analogues; see, e.g., [24] and the references therein). In order to speed up the convergence, we can use the following strategy to vary ε and τ at each step of the operator-splitting scheme:

(a) As long as $\eta\tau_n > \chi h^2$ (with $\chi \simeq 1$), take

$$\{\tau^{n+1}, \varepsilon^{n+1}\} = \xi\{\tau^n, \varepsilon^n\} \tag{4.18}$$

with $\xi \in (0,1)$.

(b) If $\eta\tau_n \leq \chi h^2$, take

$$\{\tau^{n+q}, \varepsilon^{n+q}\} = \{\tau^n, \varepsilon^n\}, \quad \forall q \geq 1. \tag{4.19}$$

Relationship (4.19) is motivated by the fact that if τ_n goes to zero too rapidly, the time integration never reaches $t = +\infty$, and thus the steady state cannot be reached in the most stringent cases. Similarly, if $\eta\tau_n << h^2$, the biharmonic term has no regularization effect anymore.

The influence of the choice of the constant C is not crucial. An appropriate choice for C leads to the most appropriate topology of the objective function, and may improve the global convergence of the algorithm.

5 A Variant with a Nonlinear Biharmonic Regularization

After dropping the indices ε and η, (3.6) reads as follows:

$$\begin{aligned} u = \arg \min_{v \in W_g^{1,4} \cap W^{2,1}(\Omega)} \Big[& \eta \int_\Omega \sqrt{1 + |\nabla^2 v|^2} \mathrm{d}\mathbf{x} + \frac{1}{2} \int_\Omega |\nabla v|^2 \, \mathrm{d}\mathbf{x} \\ & - C \int_\Omega v \mathrm{d}\mathbf{x} + \frac{1}{4\varepsilon} \int_\Omega (|\nabla v|^2 - 1)^2 \mathrm{d}\mathbf{x} \Big]. \end{aligned} \tag{5.1}$$

If u_1 is still defined by (4.2), and if $\mathbf{p} = \nabla u$, then (5.1) is equivalent to

$$\begin{aligned} \mathbf{p} = \arg \min_{\mathbf{p} \in \widetilde{\mathbf{Q}}} \Big[& \eta \int_\Omega \sqrt{1 + |\nabla \cdot \mathbf{q}|^2} \mathrm{d}\mathbf{x} + \frac{1}{2} \int_\Omega |\mathbf{q}|^2 \, \mathrm{d}\mathbf{x} \\ & - C \int_\Omega \nabla u_1 \cdot \mathbf{q} \mathrm{d}\mathbf{x} + \frac{1}{4\varepsilon} \int_\Omega (|\mathbf{q}|^2 - 1)^2 \mathrm{d}\mathbf{x} + I_\nabla(\mathbf{q}) \Big], \end{aligned} \tag{5.2}$$

where

$$\widetilde{\mathbf{Q}} = \left\{ \mathbf{q} \in L^4(\Omega)^2 \, , \, \nabla \cdot \mathbf{q} \in L^1(\Omega) \right\}.$$

In the variational form, the Euler-Lagrange equation associated with (5.2) reads as follows: Find $\mathbf{p} \in \widetilde{\mathbf{Q}}$ satisfying

$$\begin{aligned} & \eta \int_\Omega \frac{(\nabla \cdot \mathbf{p})(\nabla \cdot \mathbf{q})}{\sqrt{1 + |\nabla \cdot \mathbf{p}|^2}} \mathrm{d}\mathbf{x} + \int_\Omega \mathbf{p} \cdot \mathbf{q} \mathrm{d}\mathbf{x} - C \int_\Omega \nabla u_1 \cdot \mathbf{q} \mathrm{d}\mathbf{x} \\ & + \frac{1}{\varepsilon} \int_\Omega (|\mathbf{p}|^2 - 1) \mathbf{p} \cdot \mathbf{q} \mathrm{d}\mathbf{x} + \langle \partial I_\nabla(\mathbf{p}), \mathbf{q} \rangle = 0, \quad \forall \mathbf{q} \in \widetilde{\mathbf{Q}}, \end{aligned} \tag{5.3}$$

with $\partial I_\nabla(\cdot)$ the sub-gradient of the functional I_∇ at $\mathbf{p}$. As in Section 4, we associate with (5.3) an initial-value problem similar to (4.9), namely, to find $\mathbf{p}(t) \in \widetilde{\mathbf{Q}}$ for a.e. $t \in (0, +\infty)$ satisfying $\mathbf{p}(0) = \mathbf{p}_0$ and

$$\begin{aligned} & \int_\Omega \frac{\partial \mathbf{p}}{\partial t} \cdot \mathbf{q} \mathrm{d}\mathbf{x} + \eta \int_\Omega \frac{(\nabla \cdot \mathbf{p})(\nabla \cdot \mathbf{q})}{\sqrt{1 + |\nabla \cdot \mathbf{p}|^2}} \mathrm{d}\mathbf{x} + \int_\Omega \mathbf{p} \cdot \mathbf{q} \mathrm{d}\mathbf{x} - C \int_\Omega \nabla u_1 \cdot \mathbf{q} \mathrm{d}\mathbf{x} \\ & + \frac{1}{\varepsilon} \int_\Omega (|\mathbf{p}|^2 - 1) \mathbf{p} \cdot \mathbf{q} \mathrm{d}\mathbf{x} + \langle \partial I_\nabla(\mathbf{p}), \mathbf{q} \rangle = 0, \quad \forall \mathbf{q} \in \widetilde{\mathbf{Q}}. \end{aligned} \tag{5.4}$$

Following the approach we took in Section 4, we are going to use again an operator-splitting scheme à la Marchuk-Yanenko to solve the problem (5.4). The initialization and the solution to the local optimization problems are similar to those in Section 4. The main difference has to do with the solution of the variational problem (4.12), which now reads: Find $\mathbf{p}^{n+1} \in \widetilde{\mathbf{Q}}$

satisfying

$$\int_\Omega \frac{\mathbf{p}^{n+1}-\mathbf{p}^{n+\frac{1}{2}}}{\tau}\cdot\mathbf{q}\mathrm{d}\mathbf{x}+\eta\int_\Omega \frac{(\nabla\cdot\mathbf{p}^{n+1})(\nabla\cdot\mathbf{q})}{\sqrt{1+|\nabla\cdot\mathbf{p}^{n+1}|^2}}\mathrm{d}\mathbf{x}+\int_\Omega \mathbf{p}^{n+1}\cdot\mathbf{q}\mathrm{d}\mathbf{x}$$
$$-C\int_\Omega \nabla u_1\cdot\mathbf{q}\mathrm{d}\mathbf{x}+\left\langle\partial I_\nabla(\mathbf{p}^{n+1}),\mathbf{q}\right\rangle=0,\quad \forall\mathbf{q}\in\widetilde{\mathbf{Q}}. \tag{5.5}$$

By setting $\nabla u^{n+1}:=\mathbf{p}^{n+1}$, there is equivalence between the problem (5.5) and finding $u^{n+1}\in W^{2,1}(\Omega)\cap H^1_g(\Omega)$ that satisfy

$$\int_\Omega \frac{\nabla u^{n+1}-\mathbf{p}^{n+\frac{1}{2}}}{\tau}\cdot\nabla v\mathrm{d}\mathbf{x}+\eta\int_\Omega \frac{(\nabla^2 u^{n+1})(\nabla^2 v)}{\sqrt{1+|\nabla^2 u^{n+1}|^2}}\mathrm{d}\mathbf{x}+\int_\Omega \nabla u^{n+1}\cdot\nabla v\mathrm{d}\mathbf{x}$$
$$-C\int_\Omega v\mathrm{d}\mathbf{x}=0,\quad \forall v\in H^2(\Omega)\cap H^1_0(\Omega). \tag{5.6}$$

The problem (5.6) is nothing but the variational formulation of the following nonlinear biharmonic problem:

$$\begin{cases} -(1+\tau)\nabla^2 u^{n+1}+\eta\tau\nabla^2\dfrac{\nabla^2 u^{n+1}}{\sqrt{1+|\nabla^2 u^{n+1}|^2}}=\tau C-\nabla\cdot\mathbf{p}^{n+\frac{1}{2}} \quad \text{in } \Omega,\\ u^{n+1}=g \quad \text{on } \Gamma,\\ \nabla^2 u^{n+1}=0 \quad \text{on } \Gamma, \end{cases}$$

which is equivalent to the following system of second-order elliptic equations:

$$\begin{cases} (1+\tau)w^{n+1}-\eta\tau\nabla^2\dfrac{w^{n+1}}{\sqrt{1+|w^{n+1}|^2}}=\tau C-\nabla\cdot\mathbf{p}^{n+\frac{1}{2}} \quad \text{in } \Omega,\\ w^{n+1}=0 \quad \text{on } \Gamma, \end{cases}$$

$$\begin{cases} -\nabla^2 u^{n+1}=w^{n+1} \quad \text{in } \Omega,\\ u^{n+1}=g \quad \text{on } \Gamma. \end{cases}$$

The first of these second-order elliptic equations can be formulated in the divergence form, namely,

$$\begin{cases} (1+\tau)w^{n+1}-\eta\tau\nabla\cdot\dfrac{\nabla w^{n+1}}{(1+|w^{n+1}|^2)^{\frac{3}{2}}}=\tau C-\nabla\cdot\mathbf{p}^{n+\frac{1}{2}} \quad \text{in } \Omega,\\ w^{n+1}=0 \quad \text{on } \Gamma. \end{cases} \tag{5.7}$$

From the small size of the coefficient $\eta\tau$, it is tempting to use, in practice, the following simple linearization:

$$\begin{cases} (1+\tau)w^{n+1}-\eta\tau\nabla\cdot\dfrac{\nabla w^{n+1}}{(1+|w^{n}|^2)^{\frac{3}{2}}}=\tau C-\nabla\cdot\mathbf{p}^{n+\frac{1}{2}} \quad \text{in } \Omega,\\ w^{n+1}=0 \quad \text{on } \Gamma. \end{cases} \tag{5.8}$$

The elliptic operator in (5.8) is linear, self-adjoint and strictly positive. Using (5.8) avoids solving the nonlinear problem (5.7) by Newton's, quasi-Newton, or other methods.

Remark 5.1 If for some reason, w^0 is required (as it will be if we use (5.8) instead of (5.7)), we can take $w^0=C$.

6 Finite Element Discretization

6.1 Generalities

Finite element methods are well-suited to the solution of variational problems such as (3.5) (or (3.6)), particularly those methods relying on continuous piecewise linear approximations on triangulations of Ω. Indeed, piecewise linear finite element methods rely on spaces of Lipschitz continuous functions well-suited to the approximation of solutions to the Eikonal equation, whose regularity is precisely Lipschitz, and whose second derivatives do not have, in general, an $L^s(\Omega)$-regularity, even for $s = 1$, implying that higher-order methods will not bring additional accuracy.

Let us define a space discretization step $h > 0$, and associate with h a triangulation $\mathcal{T}_h$ that satisfies the usual compatibility conditions (see, e.g., [25] for a complete definition). Let us denote by Σ_h the (finite) set of the vertices of $\mathcal{T}_h$, by N_h the number of elements in Σ_h, and by Σ_{0h} the subset of those elements in Σ_h not located on Γ (with $N_{0h} := \mathrm{card}(\Sigma_{0h})$). From the triangulation $\mathcal{T}_h$, we define the following finite element spaces:

$$
\begin{aligned}
V_h &= \left\{ v \in C^0\left(\overline{\Omega}\right),\ v|_K \in \mathbb{P}_1,\ \forall K \in \mathcal{T}_h \right\},\\
V_{gh} &= \left\{ v \in V_h,\ v(P) = g(P),\ \forall P \in \Gamma \cap \Sigma_h \right\},\\
V_{0h} &= \left\{ v \in V_h,\ v = 0 \ \text{ on } \Gamma \right\},\\
\mathbf{Q}_h &= \left\{ \mathbf{q} \in L^\infty(\Omega)^2,\ \mathbf{q}|_K \in \mathbb{R}^2,\ \forall K \in \mathcal{T}_h \right\},
\end{aligned}
$$

where $\mathbb{P}_1$ is the space of the two-variable polynomials of degree ≤ 1. We clearly have

$$
\nabla V_h \subset \mathbf{Q}_h. \tag{6.1}
$$

With each point $P_i \in \Sigma_h$, we associate the piecewise linear basis function $\varphi_i \in V_h$, $i = 1, \cdots, N_h$, uniquely defined by $\varphi_i(P_i) = 1$, $\varphi_i(P_j) = 0$, $j = 1, \cdots, N_h$, $j \neq i$. Next, we equip V_h, and its sub-spaces V_{0h} and V_{gh} with the following discrete scalar product:

$$
(v, w)_{0h} = \frac{1}{3} \sum_{k=1}^{N_h} A_k v(P_k) w(P_k), \quad \forall v, w \in V_h,
$$

and the corresponding norm $||v||_{0h} := \sqrt{(v, v)_{0h}}$, for all $v \in V_h$; above, A_k denotes the area of the polygonal domain which is the union of those triangles of $\mathcal{T}_h$ which have P_k as a common vertex. In a similar fashion, we equip the space $\mathbf{Q}_h$ with the scalar product and the norm respectively defined as follows:

$$
((\mathbf{p}, \mathbf{q}))_{0h} = \sum_{K \in \mathcal{T}_h} |K|\ \mathbf{p}|_K \cdot \mathbf{q}|_K
$$

and $|||\mathbf{q}|||_{0h} = \sqrt{((\mathbf{q}, \mathbf{q}))_{0h}}$ (with $|K|$ = area of K).

6.2 Approximation of the regularized variational problem

After dropping the indices ε and η, we approximate the problem (3.5) by

$$
\begin{aligned}
u_h = \arg\min_{v \in V_{gh}} \Big[&\frac{\eta}{2}(\theta, \theta)_{0h} + \frac{1}{2} \int_\Omega |\nabla v|^2 \,\mathrm{d}\mathbf{x} \\
&- C \int_\Omega v \mathrm{d}\mathbf{x} + \frac{1}{4\varepsilon} \int_\Omega (|\nabla v|^2 - 1)^2 \mathrm{d}\mathbf{x} \Big],
\end{aligned} \tag{6.2}
$$

where $\theta = \theta(v) \in V_{0h}$ is defined from v via the solution of the following finite-dimensional linear variational problem:

$$\theta \in V_{0h}, \quad (\theta, \varphi)_{0h} = \int_\Omega \nabla v \cdot \nabla \varphi \mathrm{d}\mathbf{x}, \quad \forall \varphi \in V_{0h}. \tag{6.3}$$

The optimality conditions associated with (6.2)–(6.3) read as follows: Find $\{u_h, w_h\} \in V_{gh} \times V_{0h}$ such that

$$\begin{cases} \eta(w_h, v)_{0h} + \displaystyle\int_\Omega \nabla w_h \cdot \nabla v \mathrm{d}\mathbf{x} + \frac{1}{\varepsilon} \int_\Omega (|\nabla u_h|^2 - 1) \nabla u_h \cdot \nabla v \mathrm{d}\mathbf{x} = C \int_\Omega v \mathrm{d}\mathbf{x}, \\ \hfill \forall v \in V_{0h}, \\ (w_h, v)_{0h} = \displaystyle\int_\Omega \nabla u_h \cdot \nabla v \mathrm{d}\mathbf{x}, \quad \forall v \in V_{0h}. \end{cases} \tag{6.4}$$

The main difficulty with problem (6.4) is its cubic nonlinearity. In order to decouple this nonlinearity from the differential operators, we observe that (6.4) is equivalent to the following system:

$$\nabla u_h = \mathbf{p}_h, \tag{6.5}$$

$$\mathbf{p}_h = \arg \min_{\mathbf{q} \in \mathbf{Q}_h} \Big[\frac{\eta}{2} (\theta, \theta)_{0h} + \frac{1}{2} \int_\Omega |\mathbf{q}|^2 \, \mathrm{d}\mathbf{x} \\ - C \int_\Omega \nabla u_1 \cdot \mathbf{q} \mathrm{d}\mathbf{x} + \frac{1}{4\varepsilon} \int_\Omega (|\mathbf{q}|^2 - 1)^2 \mathrm{d}\mathbf{x} + I_\nabla(\mathbf{q}) \Big], \tag{6.6}$$

where $\theta = \theta(\mathbf{q})$ is obtained from $\mathbf{q}$ as the unique solution of the discrete linear variational problem:

$$\theta \in V_{0h}, \quad (\theta, v)_{0h} = \int_\Omega \mathbf{q} \cdot \nabla v \mathrm{d}\mathbf{x}, \quad \forall v \in V_{0h}. \tag{6.7}$$

In (6.6), the function u_1 is the unique solution of the discrete variational problem

$$u_1 \in V_{gh}, \quad \int_\Omega \nabla u_1 \cdot \nabla v \mathrm{d}\mathbf{x} = \int_\Omega v \mathrm{d}\mathbf{x}, \quad \forall v \in V_{0h}, \tag{6.8}$$

and the functional $I_\nabla(\cdot)$ (an indicator functional) is defined by

$$I_\nabla(\mathbf{q}) = \begin{cases} 0, & \text{if } \mathbf{q} \in \nabla V_{gh}, \\ +\infty, & \text{if } \mathbf{q} \in \mathbf{Q}_h \backslash \nabla V_{gh}. \end{cases} \tag{6.9}$$

The optimality conditions associated with this extended system (6.6)–(6.7) read as follows: Find $\{\mathbf{p}, w, \theta\} \in \mathbf{Q}_h \times V_{0h} \times V_{0h}$ such that:

$$(w, v)_{0h} = \int_\Omega \mathbf{p} \cdot \nabla v \mathrm{d}\mathbf{x}, \tag{6.10}$$

$$\eta(w, \theta)_{0h} + \int_\Omega \mathbf{p} \cdot \mathbf{q} \mathrm{d}\mathbf{x} - C \int_\Omega \nabla u_1 \cdot \mathbf{q} \mathrm{d}\mathbf{x} \\ + < \partial I_\nabla(\mathbf{p}), \mathbf{q} > + \frac{1}{\varepsilon} \int_\Omega (|\mathbf{p}|^2 - 1) \mathbf{p} \cdot \mathbf{q} \mathrm{d}\mathbf{x} = 0, \tag{6.11}$$

$$(\theta, v)_{0h} = \int_\Omega \mathbf{q} \cdot \nabla v \mathrm{d}\mathbf{x} \tag{6.12}$$

for all $\{\mathbf{q}, v\} \in \mathbf{Q}_h \times V_{0h}$.

6.3 Initial-value problem and operator-splitting

As in Subsection 4.2, we associate with (6.10)–(6.12) an initial-value problem that corresponds to a finite-dimensional flow in the dynamical system sense. The variational formulation of this initial-value problem reads as follows: Find $\{\mathbf{p}(t), w(t)\} \in \mathbf{Q}_h \times V_{0h}$, for a.e. $t \in (0, \infty)$, satisfying

$$\begin{aligned}&\int_\Omega \frac{\partial \mathbf{p}(t)}{\partial t} \cdot \mathbf{q} d\mathbf{x} + \eta(w, \theta)_{0h} + \int_\Omega \mathbf{p} \cdot \mathbf{q} d\mathbf{x} - C \int_\Omega \nabla u_1 \cdot \mathbf{q} d\mathbf{x} \\ &+ \langle \partial I_\nabla(\mathbf{p}), \mathbf{q} \rangle + \frac{1}{\varepsilon} \int_\Omega (|\mathbf{p}|^2 - 1)\mathbf{p} \cdot \mathbf{q} d\mathbf{x} = 0 \end{aligned} \tag{6.13}$$

for all $\mathbf{q} \in \mathbf{Q}_h$, together with $\theta \in V_{0h}$,

$$(\theta, v)_{0h} = \int_\Omega \mathbf{q} \cdot \nabla v d\mathbf{x}, \quad \forall v \in V_{0h}, \tag{6.14}$$

$$(w(t), v)_{0h} = \int_\Omega \mathbf{p}(t) \cdot \nabla v d\mathbf{x}, \quad \forall v \in V_{0h}, \tag{6.15}$$

and the initial condition $\mathbf{p}(0) = \mathbf{p}_0$ given in $\mathbf{Q}_h$. For the choice of $\mathbf{p}_0$, we suggest to compute first the solution of the discrete Poisson problem: Find $u_0 \in V_{gh}$ such that $\int_\Omega \nabla u_0 \cdot \nabla v d\mathbf{x} = C \int_\Omega v d\mathbf{x}$ for all $v \in V_{0h}$ and then set

$$\forall K \in \mathcal{T}_h, \quad \mathbf{p}_0|_K = \begin{cases} \frac{\nabla u_0|_K}{|\nabla u_0|_K|}, & \text{if } \nabla u_0|_K \neq \mathbf{0}, \\ \mathbf{0}, & \text{if } \nabla u_0|_K = \mathbf{0}. \end{cases}$$

Let $\tau(> 0)$ be the time-discretization step. To time-discretize the initial-value problem (6.13)–(6.14), we advocate the following Marchuk-Yanenko-type scheme: Starting with $\mathbf{p}^0 = \mathbf{p}_0$, we compute $\mathbf{p}^{n+1}$ from $\mathbf{p}^n$, for $n \geq 0$, via the following time-splitting scheme:

1. Solve the discrete nonlinear problem: Find $\mathbf{p}^{n+\frac{1}{2}}$ such that

$$\int_\Omega \frac{\mathbf{p}^{n+\frac{1}{2}} - \mathbf{p}^n}{\tau} \cdot \mathbf{q} d\mathbf{x} + \frac{1}{\varepsilon} \int_\Omega (|\mathbf{p}^{n+\frac{1}{2}}|^2 - 1)\mathbf{p}^{n+\frac{1}{2}} \cdot \mathbf{q} d\mathbf{x} = 0 \tag{6.16}$$

for all $\mathbf{q} \in \mathbf{Q}_h$.

2. Solve the discrete variational problem: Find $\{\mathbf{p}^{n+1}, w^{n+1}\} \in \mathbf{Q}_h \times V_{0h}$ such that

$$\begin{aligned}&\int_\Omega \frac{\mathbf{p}^{n+1} - \mathbf{p}^{n+\frac{1}{2}}}{\tau} \cdot \mathbf{q} d\mathbf{x} + \eta(w^{n+1}, \theta)_{0h} + \int_\Omega \mathbf{p}^{n+1} \cdot \mathbf{q} d\mathbf{x} \\ &- \int_\Omega \nabla u_1 \cdot \mathbf{q} d\mathbf{x} + \langle \partial I_\nabla(\mathbf{p}^{n+1}), \mathbf{q} \rangle = 0, \quad \forall \{\mathbf{q}, \theta\} \in \mathbf{Q}_h \times V_{0h}, \end{aligned} \tag{6.17}$$

together with

$$(w^{n+1}, v)_{0h} = \int_\Omega \mathbf{p}^{n+1} \cdot \nabla v d\mathbf{x}, \quad (\theta, v)_{0h} = \int_\Omega \mathbf{q} \cdot \nabla v d\mathbf{x}, \quad \forall v \in V_{0h}. \tag{6.18}$$

Remark 6.1 Let us introduce $\mathbf{p}^{n+1} = \nabla u^{n+1}$; there is then equivalence between system (6.17)–(6.18) and finding $\left\{u^{n+1}, w^{n+1}\right\} \in V_{gh} \times V_{0h}$ that satisfy

$$\begin{aligned}&\tau\eta \int_\Omega \nabla w^{n+1} \cdot \nabla v d\mathbf{x} + (1 + \tau)(w^{n+1}, v)_{0h} = \int_\Omega \mathbf{p}^{n+\frac{1}{2}} \cdot \nabla v d\mathbf{x} + \tau C \int_\Omega v d\mathbf{x}, \\ &\int_\Omega \nabla u^{n+1} \cdot \nabla v d\mathbf{x} = (w^{n+1}, v)_{0h}\end{aligned}$$

both for all $v \in V_{0h}$.

6.4 On the solution of the discrete nonlinear problems

The finite-dimensional nonlinear problem (6.16) can be solved triangle-wise; indeed, if we denote $\mathbf{q}|_K$ by $\mathbf{q}_K$, we can rewrite (6.16) as follows: Find $\mathbf{p}^{n+\frac{1}{2}} := \{\mathbf{p}_K^{n+\frac{1}{2}}\}_{K\in\mathcal{T}_h}$ satisfying

$$\mathbf{p}_K^{n+\frac{1}{2}}\left[\frac{\tau}{\varepsilon}|\mathbf{p}_K^{n+\frac{1}{2}}|^2 + \left(1-\frac{\tau}{\varepsilon}\right)\right] = \mathbf{p}_K^n, \quad \forall K \in \mathcal{T}_h. \tag{6.19}$$

Let us assume from now on that $\varepsilon \geq \tau$; under this assumption, we observe that $|\mathbf{p}_K^{n+\frac{1}{2}}|$ is the unique solution of the cubic one-variable equation:

$$\frac{\tau}{\varepsilon}\rho^3 + \left(1-\frac{\tau}{\varepsilon}\right)\rho - |\mathbf{p}_K^n| = 0, \quad \forall K \in \mathcal{T}_h. \tag{6.20}$$

The Newton's method can be applied to the solution of (6.20). Once the $|\mathbf{p}_K^{n+\frac{1}{2}}|$ are known, we obtain $\mathbf{p}_K^{n+\frac{1}{2}}$ from

$$\mathbf{p}_K^{n+\frac{1}{2}} = \frac{\mathbf{p}_K^n}{\frac{\tau}{\varepsilon}|\mathbf{p}_K^{n+\frac{1}{2}}|^2 + \left(1-\frac{\tau}{\varepsilon}\right)}, \quad \forall K \in \mathcal{T}_h. \tag{6.21}$$

6.5 Further comments

The discrete linear variational problem (6.17)–(6.18) is of the mixed type; it consists of two discrete elliptic problems, each of them being equivalent to a linear system associated with a matrix which is sparse, symmetric and positive definite. A large variety of solution methods exists for such systems, while among them are the fast elliptic solvers of FISHPACK if the mesh is uniform, and the sparse Cholesky solvers, like those available in MATLAB. Clearly, the approximation methods discussed in Subsections 6.1–6.4 can be easily modified in order to handle the numerical solution of the nonlinearly regularized problem (5.1) via the operator-splitting scheme (5.5)–(5.6).

7 Numerical Experiments

In this section, we will present the results of numerical experiments. Most of them are concerned (not surprisingly) with the particular case where $\Omega = (0,1)^2$, however, test problems where Ω has a (totally or partially) curved boundary or where Ω is not convex will also be considered. The finite element triangulations we use are either structured or isotropic à la Delaunay. All the experiments have been performed on an Intel Xeon computer (2.93 GHz) with 8 GB memory. The results have been post-processed with Paraview.

7.1 Solution of the Eikonal equation with homogeneous boundary conditions on the unit square (recovery of the distance function)

Let us consider $\Omega = (0,1)^2$. The first numerical example corresponds to the homogeneous case $g = 0$ in (2.1). The maximal solution to (2.1) is clearly the distance function $\mathbf{x} \to \delta(\mathbf{x}, \Gamma)$ (distance of $\mathbf{x}$ to the boundary Γ of Ω); it is given here by

$$u_{\max}(x_1, x_2) = \min\{x_1, 1-x_1, x_2, 1-x_2\}, \quad \forall \mathbf{x} = (x_1, x_2) \in \Omega. \tag{7.1}$$

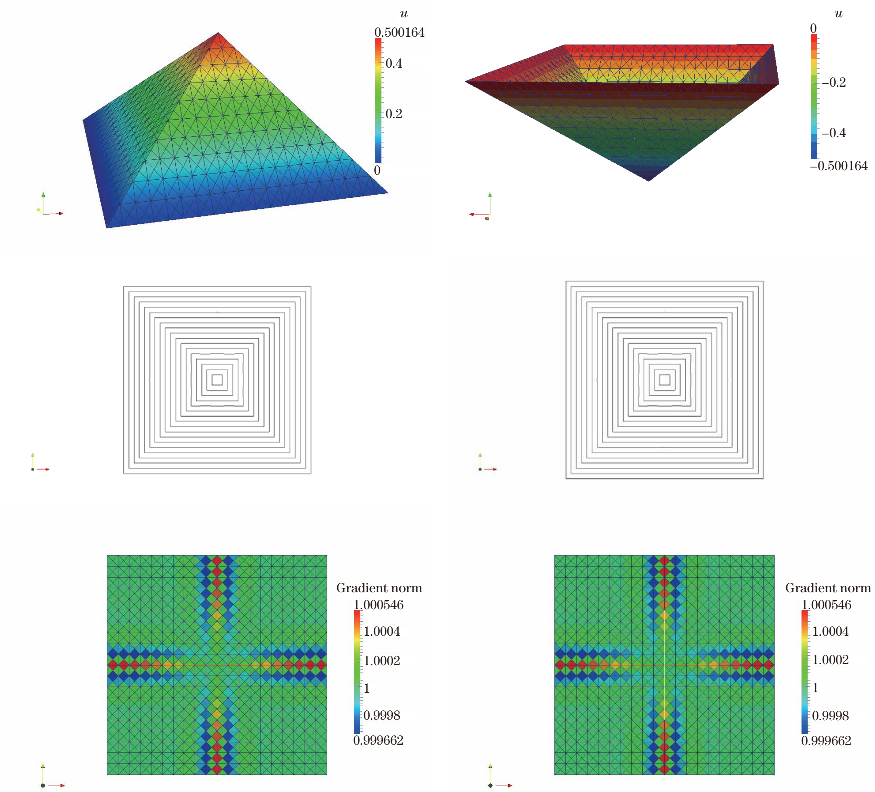

Figure 1 Distance function on the unit square ($g = 0$). Approximation u_h of the solution of the Eikonal equation ($h = \frac{1}{20}$, after 100 iterations). Left: Maximal solution; right: Minimal solution. First row: Graph of u_h, second row: Contours of u_h, third row: Piecewise constant approximation of $|\nabla u_h|$.

Since $g = 0$, the minimal solution of (2.1) is just the opposite of the maximal one, i.e. $u_{\min} = -u_{\max}$. For our computations, we have used the strategy with variable ε and τ as described in (4.18) and (4.19), with $\varepsilon^0 = 0.1$, $\tau^0 = 0.09$, $\xi = 0.9$, and the other parameters being $\eta = 0.1$ and $C = 10$. The finite element mesh we use is a structured triangulation $\mathcal{T}_h$ of the "British flag" type where h denotes the length of the edges adjacent to the right angles. For the solution of the local nonlinear 2×2 systems, we have used the Newton's method with the stopping criterion tolerance equal to 10^{-4}; with this tolerance, the Newton's algorithm was always converging in less than 10 iterations, typically.

In Figure 1, we have reported, using linear biharmonic regularization, the graph of the computed maximal and minimal solutions, their contours, and the "contours" of $|\nabla u_{\max,h}|$ and $|\nabla u_{\min,h}|$ obtained with $h = \frac{1}{20}$ and 100 iterations (in fact, 100-time steps of the operator-splitting scheme (6.16)–(6.18)). Numerically, we also obtain $u_{\min,h} = -u_{\max,h}$. As an indication, the maximal value for $u_{\max,h}$ is 0.500164 for $h = \frac{1}{20}$, 0.500211 for $h = \frac{1}{30}$, and 0.500228 for $h = \frac{1}{40}$, which are accurate approximations of the maximal value of $u_{\max}$, which is 0.5. These results show that the Eikonal equation is satisfied, up to rounding errors and mesh effects (indeed, $0.999662 \leq |\nabla u_{\max,h}| = |\nabla u_{\min,h}| \leq 1.000546$, a.e. on Ω if $h = \frac{1}{20}$).

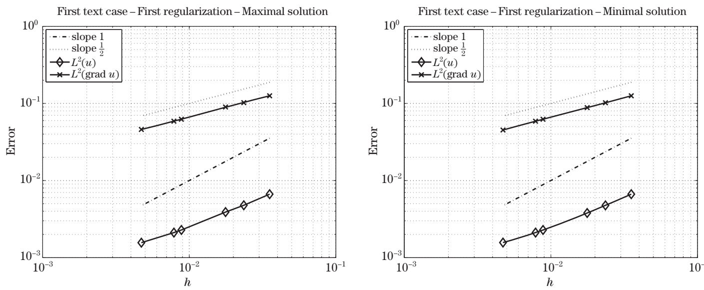

Figure 2 Computed distance function on the unit square ($g = 0$; linear biharmonic regularization). Approximation errors $||u_h - u_{\min}||_{0h}$ and $||\nabla(u_h - u_{\min})||$ (resp. $||u_h - u_{\max}||_{0h}$ and $||\nabla(u_h - u_{\max})||$) versus h (100 outer iterations). Left: Maximal solution; right: Minimal solution.

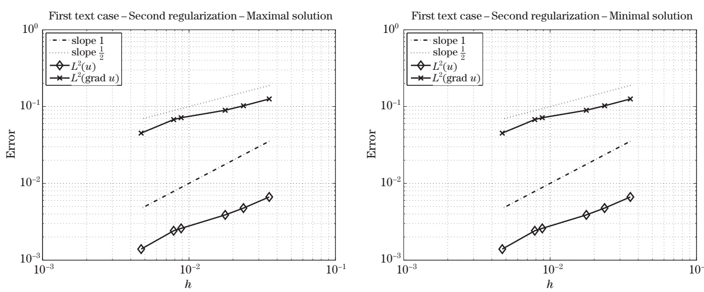

Figure 3 Computed distance function on the unit square ($g = 0$; nonlinear biharmonic regularization). Approximation errors $||u_h - u_{\min}||_{0h}$ and $||\nabla(u_h - u_{\min})||$ (resp. $||u_h - u_{\max}||_{0h}$ and $||\nabla(u_h - u_{\max})||$) versus h (100 outer iterations). Left: Maximal solution; right: Minimal solution.

Convergence results are visualized in Figure 2; they show the $\mathcal{O}(h^{\frac{1}{2}})$ approximation error for both the L^2 and H^1-norms, whenever $u = u_{\max}$ or $u = u_{\min}$. The low regularity of the solution (they belong to $W^{1,\infty}(\Omega) \cap H^s(\Omega)$ for all $s < \frac{3}{2}$) explains why we do not obtain the usual $\mathcal{O}(h^2)$ and $\mathcal{O}(h)$ approximation errors.

If we use the nonlinear biharmonic regularization discussed in Section 5, we obtain numerical results very close to those obtained with the linear regularization from Sections 3–4. The related convergence results are shown in Figure 3: they are close to those obtained with the linear regularization and thus the difference does not warrant further comparisons.

Remark 7.1 The various numerical experiments we have performed in this article show that if they can be employed (which is definitely the case with square domains), "British flag"-type meshes behave quite well compared with other types of triangulations. This is in strong contrast with what we observed when solving, also via a nonlinear biharmonic approach, the elliptic Monge-Ampère equation $\det \mathbf{D}^2 u = f$ (with $f > 0$, $\mathbf{D}^2 u$ being the Hessian of u); indeed for this fully nonlinear elliptic equation, the worst numerical results were obtained with "British flag" triangulations (see [6] for details).

There is nothing mysterious about these different behaviors: Indeed, for the Eikonal equation discussed here, the biharmonic terms $\nabla^4 u$ and $\nabla^2 \frac{\nabla^2 u}{\sqrt{1+|\nabla^2 u|^2}}$ have been introduced for smoothing purposes, being multiplied by a small coefficient (of the order of h^2 for their discrete analogues); on the other hand, when solving the above Monge-Ampère equation, the discrete second-order derivatives associated with "British flag" triangulations are very poor approximations of their continuous counterparts, explaining the bad results they produce.

7.2 Solution of the Eikonal equation with homogeneous boundary conditions on two-dimensional domains with curved boundary (recovery of the distance function)

If $g = 0$, the maximal solution to (2.1) is the distance to the boundary function, whatever the (convex) domain Ω is (see, e.g., [12]). We consider here the following two-dimensional domains, namely, the unit disk, an ellipse of axes of length 1 and 2, and the half-disk. The values of the numerical parameters are the same as in Subsection 7.1, except C that we take equal to 500 here. In Figure 4 (the top row), we have reported the graph of the computed approximations u_h of the distance function for the three domains above using the linear biharmonic regularization. There is no doubt that using piecewise linear approximations greatly facilitates the solution of the Eikonal equation (2.1) on domains with curved boundary (see also [6]). In Figure 4 (the bottom row), we have visualized $|\nabla u_h|$: The relation $|\nabla u_h| = 1$ is accurately verified, the discrepancies being very localized (along edges and at corners, in particular); this behavior was expected, but overall the numerical results we obtained show the robustness of our approach. In Figure 5, in the particular case of the unit disk, we have visualized the convergence properties of the computed approximate solutions obtained by using both the linear and nonlinear biharmonic regularizations: Both regularizations produce essentially the same results, suggesting $\mathcal{O}(h^{\frac{1}{2}})$ for both $||u_h - u||_{0h}$ and $||\nabla(u_h - u)||$.

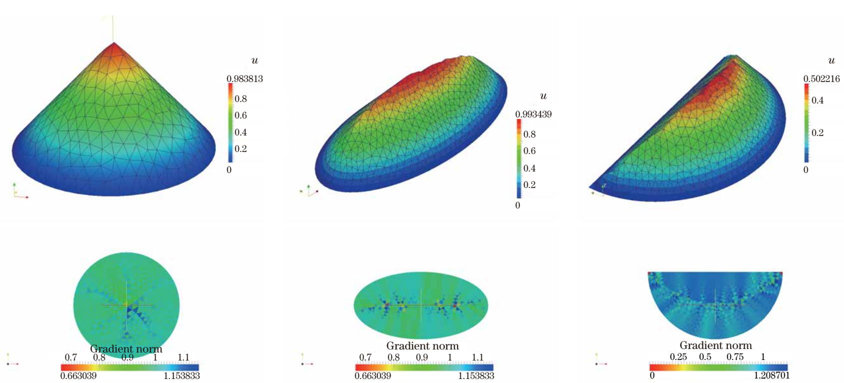

Figure 4 Computed distance function on domains Ω with curved boundaries ($g = 0$, linear biharmonic regularization). Approximation u_h of the solution of the Eikonal equation ($h = \frac{1}{20}$, after 100 iterations). Top: Graphs of the computed maximal solutions u_h. Bottom: Visualization of $|\nabla u_h|$.

Actually, for the (upper) half-disk domain, the exact maximal solution is given by

$$u_{\max}(x_1, x_2) = \min\left(1 - \sqrt{x_1^2 + x_2^2}, x_2\right), \tag{7.2}$$

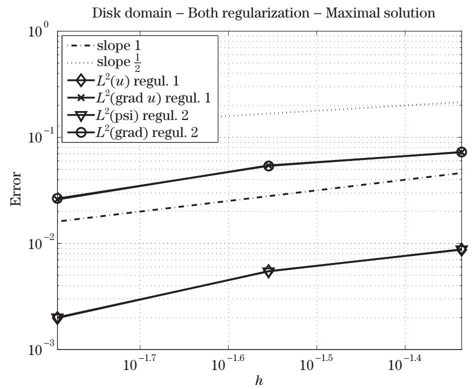

Figure 5 Computed distance function of the unit disk ($g = 0$, linear and nonlinear biharmonic regularizations). Approximation errors $||u_h - u_{\max}||_{0h}$ and $||\nabla(u_h - u_{\max})||$ versus h. Number of iterations: 100.

the ridge being the curvilinear arc whose equation, in polar coordinates, is given by

$$\rho = \frac{1}{1 + \sin(\theta)} \tag{7.3}$$

with $\theta \in [0, \pi]$. This function takes a maximal value of $\frac{1}{2}$ at the point $\left(0, \frac{1}{2}\right)$. Figure 6 (left) visualizes the order of convergence of the L^2-norm of the approximation error, while Figure 6 (right) visualizes the error on the maximum value, that is $||u_h|_\infty - 0.5|$. Both display an approximation error of order h^2, suggesting some kind of super-convergence in this particular case.

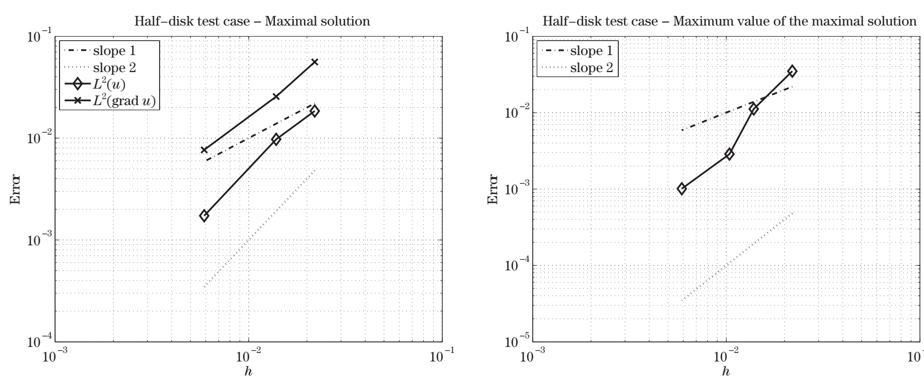

Figure 6 Computed distance function of the half-disk ($g = 0$). Approximation errors $||u_h - u_{\max}||_{0h}$ (left) and $||u_h| - 0.5|$ (right) versus h. Number of iterations: 200.

7.3 Solution of the Eikonal equation with non-homogeneous boundary conditions on the unit square (I)

The numerical example we consider now concerns the search of the maximal and minimal solutions of the Eikonal equation (2.1) when $\Omega = (0,1)^2$ and g is defined by

$$g(x_1, x_2) = \begin{cases} 0 & \text{on } \Gamma_1 \cup \Gamma_3 \cup \Gamma_4, \\ \min(x_2, 1 - x_2) & \text{on } \Gamma_2, \end{cases}$$

where $\Gamma_1 = [0,1] \times \{0\}$, $\Gamma_2 = \{1\} \times (0,1)$, $\Gamma_3 = [0,1] \times \{1\}$ and $\Gamma_4 = \{0\} \times (0,1)$. The corresponding maximal solution is given by

$$u_{\max}(x_1, x_2) = \min(x_1, x_2, 1 - x_2). \tag{7.4}$$

On the other hand, the closed form of the minimal solution is given by

$$u_{\min}(x_1, x_2) = \max\Big(- x_1, -x_2, x_2 - 1, \frac{1}{2} - \sqrt{(x_1 - 1)^2 + \Big(x_2 - \frac{1}{2}\Big)^2}\Big). \tag{7.5}$$

In order to solve numerically this new test problem, we have taken (i) $\varepsilon_0 = 0.25$, $\tau_0 = 0.2$, $\eta = 10^{-3}$, $C = 10$ and $\xi = 0.9$ if $h = \frac{1}{40}$, and (ii) $\varepsilon_0 = 0.25$, $\tau_0 = 0.2$, $\eta = 10^{-3}$, $C = 100$ and $\xi = 0.9$ if $h = \frac{1}{120}$. The mesh used is a structured mesh where the square cells are split into two triangles according to the first diagonal. When calculating the minimal solutions, parameters are identical except that $C = -100$. Figures 7–8 visualize the maximal and minimal solutions respectively. For instance, the maximal solution reaches a maximal value of 0.503278 instead of the theoretical value of 0.5 $\big($when $h = \frac{1}{50}\big)$.

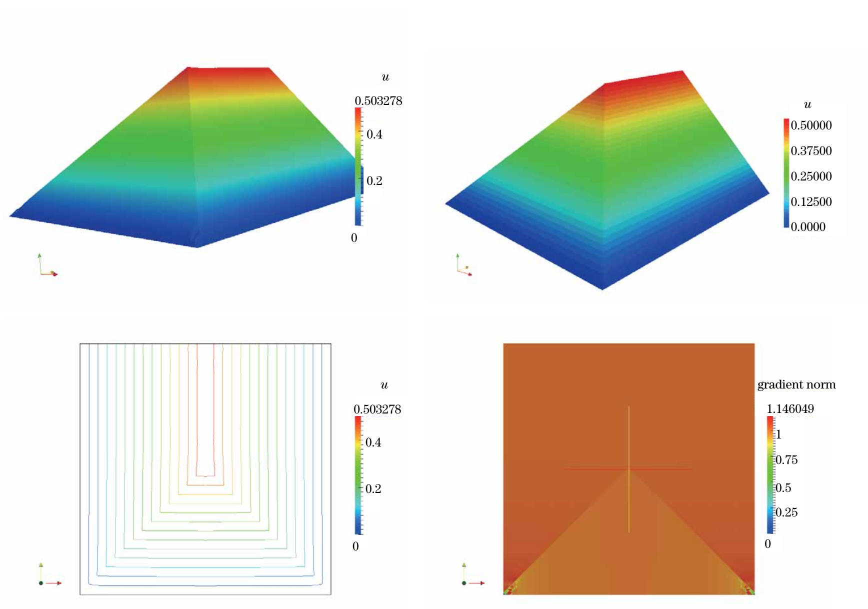

Figure 7 Non-homogeneous boundary conditions on the unit square (I). Approximation u_h of the maximal solution of the Eikonal equation $\big(h = \frac{1}{150}$, after 500 iterations$\big)$. Top left: Graph of u_h; top right: Graph of u; bottom left: Contour of $|u_h|$; bottom right: Visualization of $|\nabla u_h|$.

Looking at the gradient $|\nabla u_h|$, one can observe that it is almost everywhere equal to one. The exception is in the neighborhood of an edge, due to the mesh effects. Note that for the

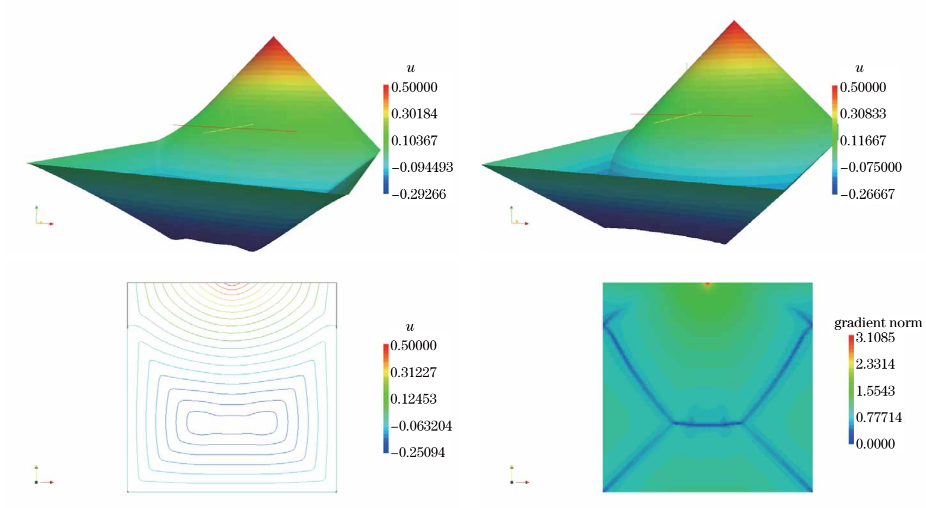

Figure 8 Non-homogeneous boundary conditions on the unit square (I). Approximation u_h of the minimal solution of the Eikonal equation $\left(h = \frac{1}{150}\right.$, after 700 iterations$\left.\right)$. Top left: Graph of u_h; top right: Graph of u; bottom left: Contour of $|u_h|$; bottom right: Visualization of $|\nabla u_h|$.

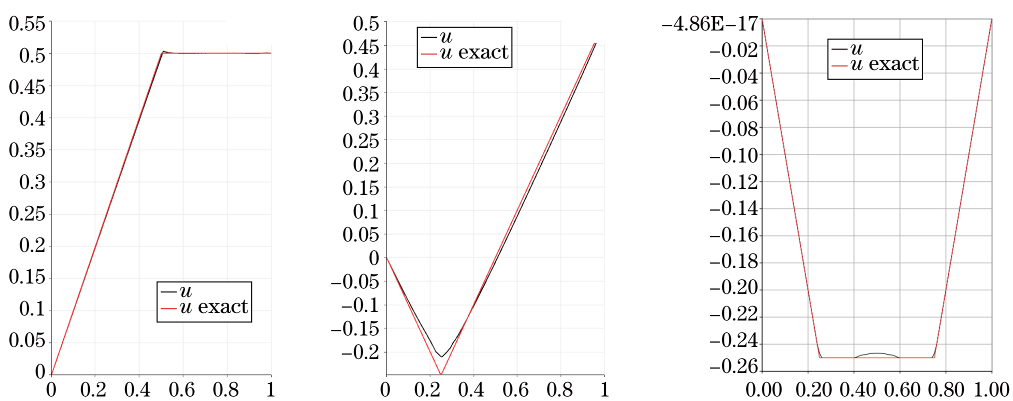

Figure 9 Non-homogeneous boundary conditions on the unit square (I) (linear biharmonic regularization). Approximation u_h of the solution of the Eikonal equation. Left: Maximal solution, cut along Ox_1 at $x_2 = \frac{1}{2}$; middle: Minimal solution, cut along Ox_1 at $x_2 = \frac{1}{2}$; right: Minimal solution, cut along Ox_2 at $x_1 = \frac{1}{4}$ $\left(h = \frac{1}{150}\right.$ –black– exact solution –red–, after 500 iterations$\left.\right)$.

maximal solution for instance, the approximation error due to the mesh is only present when mesh edges are perpendicular to the solution's ridges.

Figure 9 shows cuts of the graph of the maximal and minimal solutions for the approximation solution and the exact solution (interpolated on the same mesh). The cut of the maximal solution (left) shows that as expected, the discrepancy between the exact and computed maximal solutions is maximal at $\left(\frac{1}{2}, \frac{1}{2}\right)$, the point where the three lines of discontinuity of $\nabla u_{\max}$ encounter.

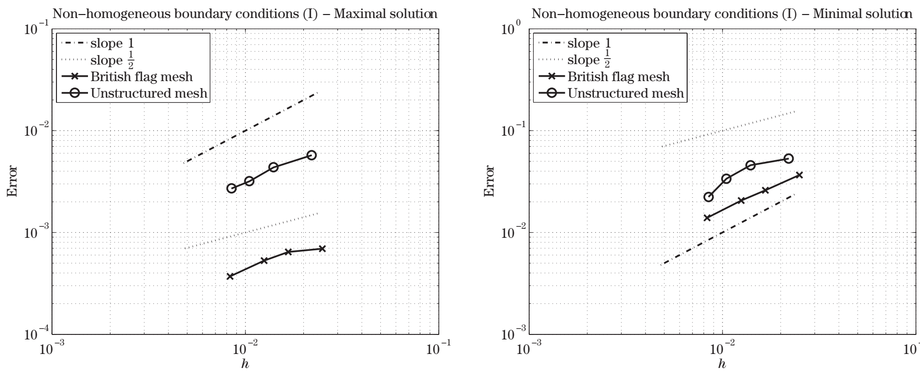

Figure 10 Non-homogeneous boundary conditions on the unit square (I) (linear biharmonic regularization). Approximation errors $||u_h - u_{\min}||_{0h}$ (resp. $||u_h - u_{\max}||_{0h}$) versus h for various types of discretizations ("British-flag" mesh and unstructured mesh). Left: Maximal solution; right: Minimal solution.

The cuts of the minimal solution show that along the Ox_1 direction, the approximation is close to the exact solution with a little diffusion effect. Along the Ox_2 direction, one sees that the approximation is more diffusive.

Figure 10 visualizes the convergence properties of the computed approximate solutions obtained on various types of discretizations of the unit square using the linear biharmonic regularization. We consider the "British flag" discretization, and a Delaunay discretization ("unstructured mesh"). All types of meshes produce essentially the same results, suggesting $\mathcal{O}(h^{\frac{1}{2}})$ for $||u_h - u||_{0h}$. When the edges of the mesh follows the lines of discontinuity of the gradient of the solution, the convergence order is actually closer from $\mathcal{O}(h)$, suggesting some kind of super convergence, a property that was expected.

7.4 Solution of the Eikonal equation with non-homogeneous boundary conditions on the unit square (II)

This numerical example corresponds to the following boundary conditions:

$$g(x_1, x_2) = \begin{cases} \min(x_1, 1 - x_1) & \text{on } \Gamma_1 \cup \Gamma_3, \\ \min(x_2, 1 - x_2) & \text{on } \Gamma_2 \cup \Gamma_4, \end{cases}$$

where $\Gamma_1 = [0,1] \times \{0\}$, $\Gamma_2 = \{1\} \times (0,1)$, $\Gamma_3 = [0,1] \times \{1\}$ and $\Gamma_4 = \{0\} \times (0,1)$. The maximal and minimal solutions are respectively given by:

$$u_{\max}(x_1, x_2) = \min\Big\{\sqrt{x_1^2 + x_2^2}\,, \sqrt{(x_1-1)^2 + x_2^2}\,, \sqrt{x_1^2 + (x_2-1)^2}\,, \sqrt{(x_1-1)^2 + (x_2-1)^2}\Big\} \tag{7.6}$$

and

$$
\begin{aligned}
u_{\min}(x_1,x_2) = \max\Big\{ &\frac{1}{2} - \sqrt{x_1^2 + \Big(x_2 - \frac{1}{2}\Big)^2}\,, \\
&\frac{1}{2} - \sqrt{(x_1-1)^2 + \Big(x_2 - \frac{1}{2}\Big)^2}\,, \\
&\frac{1}{2} - \sqrt{\Big(x_1 - \frac{1}{2}\Big)^2 + x_2^2}\,, \\
&\frac{1}{2} - \sqrt{\Big(x_1 - \frac{1}{2}\Big)^2 + (x_2-1)^2}\Big\}.
\end{aligned} \tag{7.7}
$$

Note that these solutions of the closed form are identified after looking at the numerical results obtained by our method, showing once again that numerical investigations can be useful in order to determine exact solutions. They are consistent with the results of Caffarelli and Crandall [7] who show that, away from the singularities of ∇u, the solutions of the Eikonal equation $|\nabla u| = 1$ are piecewise affine or conical. Numerical parameters are the same as those used for the test case with non-homogeneous boundary conditions (I). Figures 11 and 12 visualize the maximal and minimal solutions respectively, for two different (coarse and fine) mesh discretizations. This test case is the most stringent one in terms of convergence behavior. Figure 13 illustrates cuts of the graph of the minimal or maximal solutions for the approximation solution and the exact solution (interpolated on the same mesh). These cuts show that the solution is well approximated, except for mesh effects (for instance, along the diagonal line where the ridge is perpendicular to the mesh edges).

Studying $u_{\max}$, we observe that the maximal value is reached at $(0.5, 0.5)$ with a value of $\frac{1}{\sqrt{2}}$, which is close to the values obtained by the numerical approximations. Concerning $u_{\min}$, its minimal value is zero and is also obtained at $(0.5, 0.5)$; here again the numerical approximation agrees with the exact solution.

Figure 14 visualizes the convergence properties of the computed approximate solutions obtained for the various types of discretizations of the unit square using the linear biharmonic regularization. These results suggest a convergence order for the error $||u_h - u||_{0h}$ that is between $\mathcal{O}(h^{\frac{1}{2}})$ and $\mathcal{O}(h)$. Here, the "British flag" mesh allows to track more accurately the edges of the solution (i.e., the lines of discontinuity of the gradient of the solution) than the asymmetric mesh that is oriented along one diagonal. The more general, unstructured mesh actually performs also better than the asymmetric mesh in that regard. A clear mesh effect is thus observed for the convergence orders.

Remark 7.2 When (2.1) is replaced by

$$
\begin{cases}
\Big|\dfrac{\partial u}{\partial x_1}\Big| = \Big|\dfrac{\partial u}{\partial x_2}\Big| = 1 & \text{a.e. in } \Omega, \\
u = g & \text{on } \Gamma,
\end{cases} \tag{7.8}
$$

as in [5, 12] for instance, the minimal and maximal solutions can be described analytically in a relatively simple fashion:

$$
u_{\max}(x_1,x_2) = \min(x_1, 1-x_1) + \min(x_2, 1-x_2)
$$

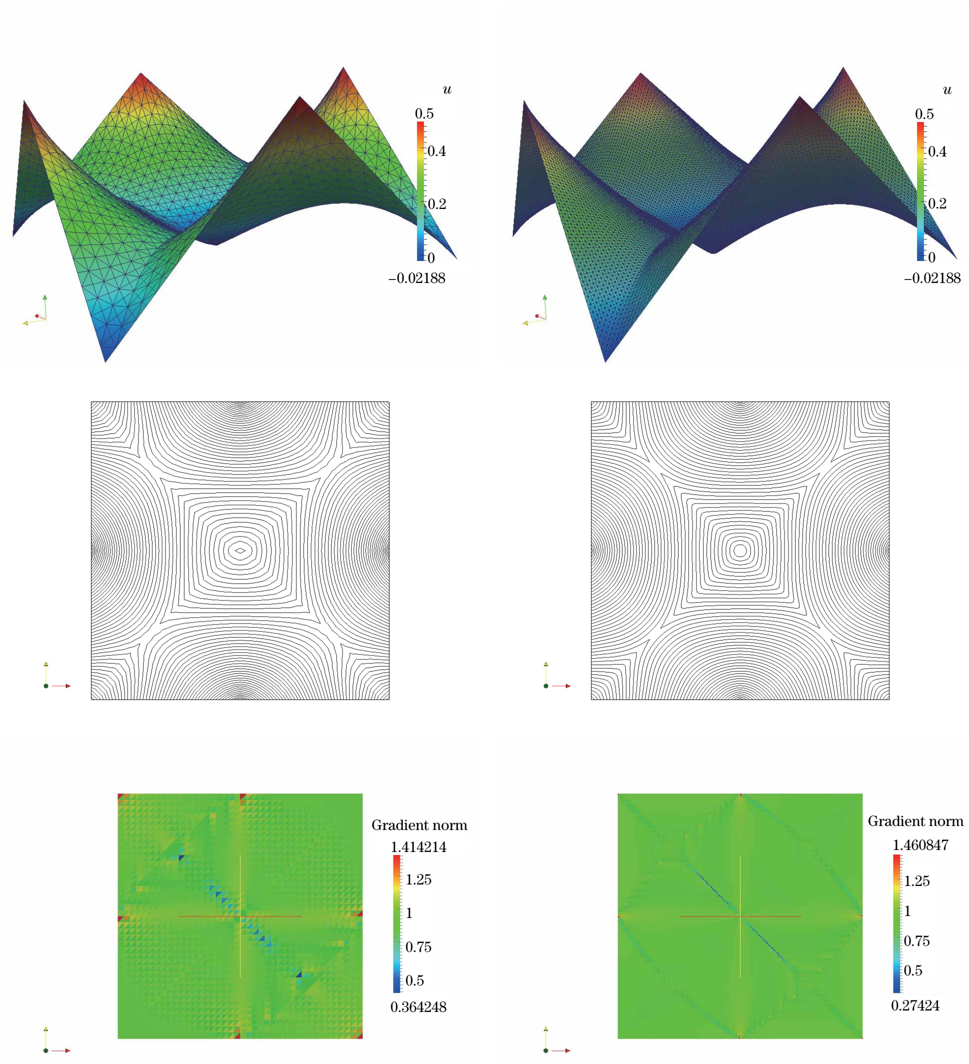

Figure 11 Non-homogeneous boundary conditions on the unit square (II); minimal solution. Approximation u_h of the solution of the Eikonal equation (after 100 iterations). Left: $h = \frac{1}{40}$; right: $h = \frac{1}{150}$. First row: Graph of u_h; second row: Contours of the graph; third row: Piecewise constant approximation ∇u_h.

and

$$u_{\min}(x_1, x_2) = \begin{cases} |x_1 - x_2|, & \text{if } 0 \le x_1, x_2 \le \dfrac{1}{2} \text{ or } \dfrac{1}{2} \le x_1, x_2 \le 1, \\ |1 - x_1 - x_2|, & \text{if } \dfrac{1}{2} \le x_1 \le 1,\ 0 \le x_2 \le \dfrac{1}{2} \text{ or } 0 \le x_1 \le \dfrac{1}{2},\ \dfrac{1}{2} \le x_2 \le 1. \end{cases}$$

This stresses out clearly some obvious difference between the solution of (2.1) and that of (7.8), for the same domain and boundary data.

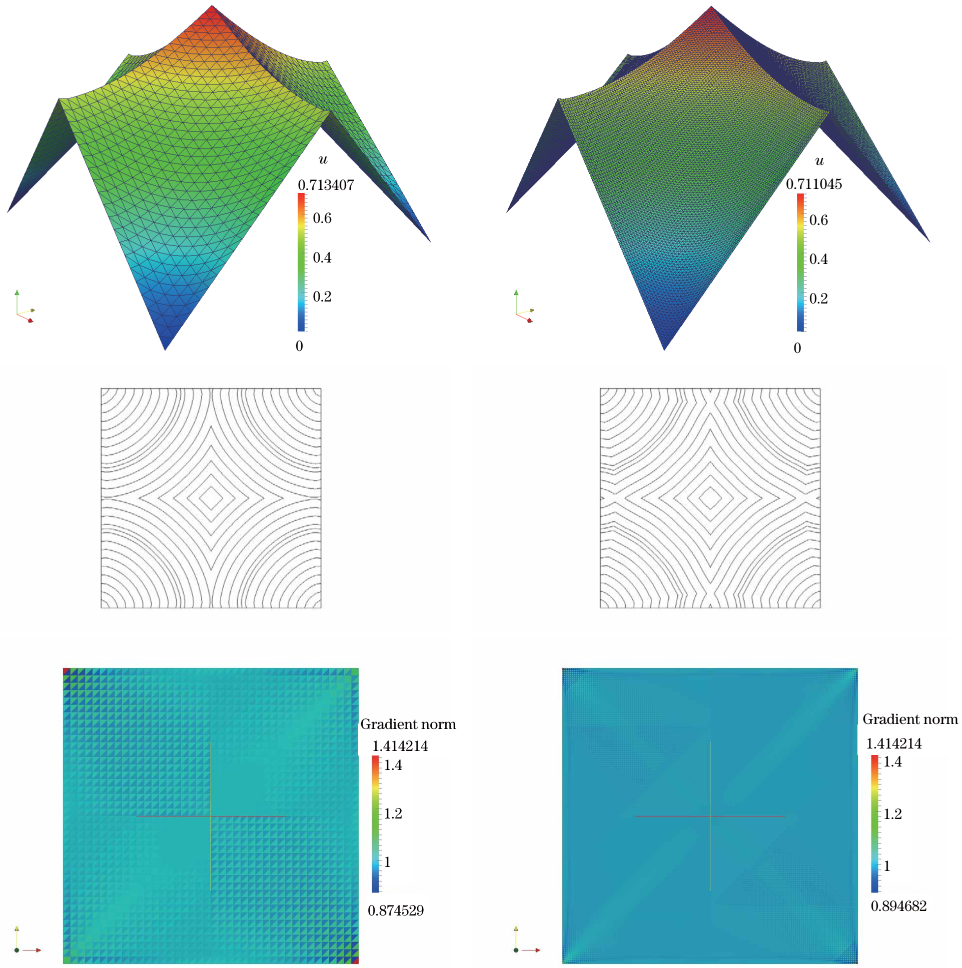

Figure 12 Non-homogeneous boundary conditions on the unit square (II); maximal solution. Approximation u_h of the solution of the Eikonal equation (after 100 iterations). Left: $h = \frac{1}{40}$; right: $h = \frac{1}{150}$. First row: Graph of u_h; second row: Contours of the graph; third row: Piecewise constant approximation ∇u_h.

7.5 Solution of the Eikonal equation with non-homogeneous boundary conditions on the unit square (III): Incompatible boundary conditions

This numerical example corresponds to the following boundary conditions:

$$g(x_1, x_2) = \begin{cases} 0 & \text{on } \Gamma_1 \cup \Gamma_3 \cup \Gamma_4, \\ \lambda \sin(\pi x_2) & \text{on } \Gamma_2, \end{cases}$$

where $\Gamma_1 = [0,1] \times \{0\}$, $\Gamma_2 = \{1\} \times (0,1)$, $\Gamma_3 = [0,1] \times \{1\}$ and $\Gamma_4 = \{0\} \times (0,1)$, and $\lambda = \frac{1}{2\pi}$ is a constant less than $\frac{1}{\pi}$. The maximal and minimal solutions are not analytically known, and the boundary conditions do not satisfy the assumptions in [7]. In particular, the function $g|_{\Gamma_2}$ not being piecewise affine or parabolic, it cannot be the trace of a solution of the Eikonal equation (2.1). Figure 15 visualizes the maximal and minimal solutions, as well as their

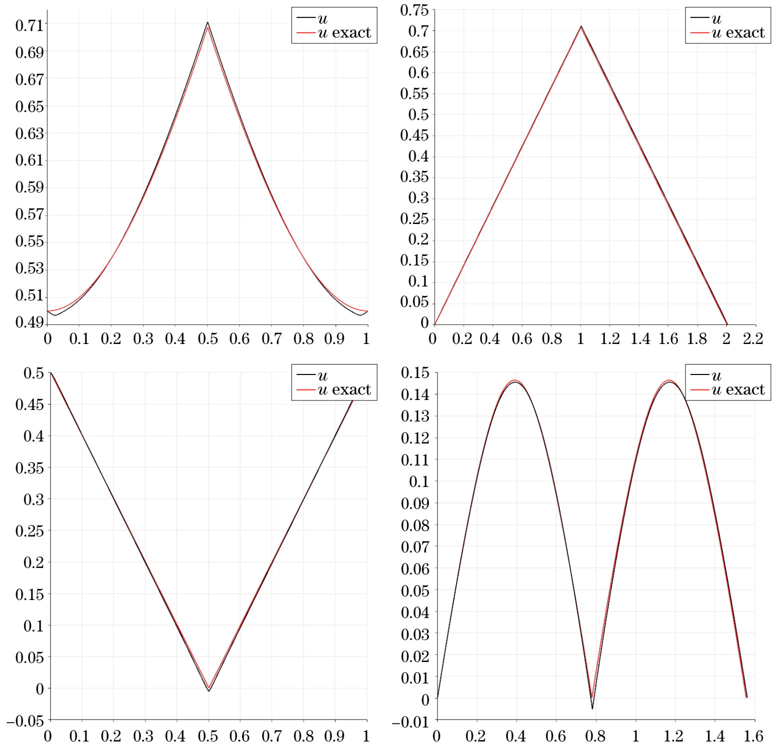

Figure 13 Non-homogeneous boundary conditions on the unit square (II). Approximation u_h of the solution of the Eikonal equation on the structured asymmetric mesh. Top row: Maximal solution: Cut along Ox_1 at $y = \frac{1}{2}$ (left); cut along the diagonal $x_1 = x_2$ (right). Bottom row: Minimal solution: Cut along Ox_1 at $y = \frac{1}{2}$ (left); cut along the diagonal $x_1 = x_2$ (right). $\left(h = \frac{1}{120}\right.$ –black– and exact solution –red–, after 100 iterations$\left.\right)$

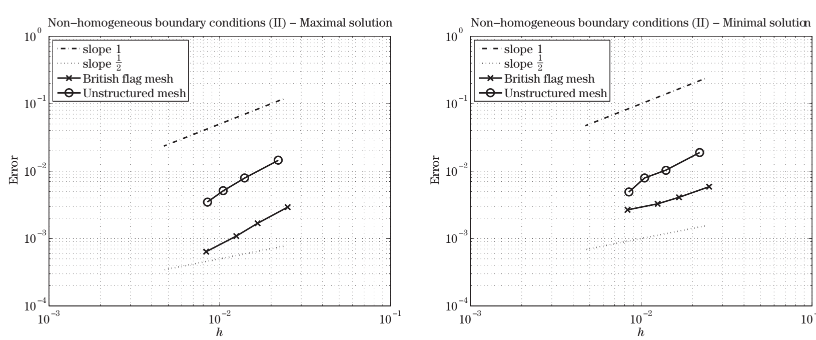

Figure 14 Non-homogeneous boundary conditions on the unit square (II) (linear biharmonic regularization). Approximation errors $||u_h - u_{\min}||_{0h}$ (resp. $||u_h - u_{\max}||_{0h}$) versus h for various types of discretizations (asymmetric structured mesh, "British-flag" mesh, and unstructured mesh). Left: Maximal solution; right: Minimal solution.

contours and the corresponding gradients. One can observe that except in a boundary layer in a neighborhood of Γ_2, in particular, around the corners of Ω, the solution is a union of cones

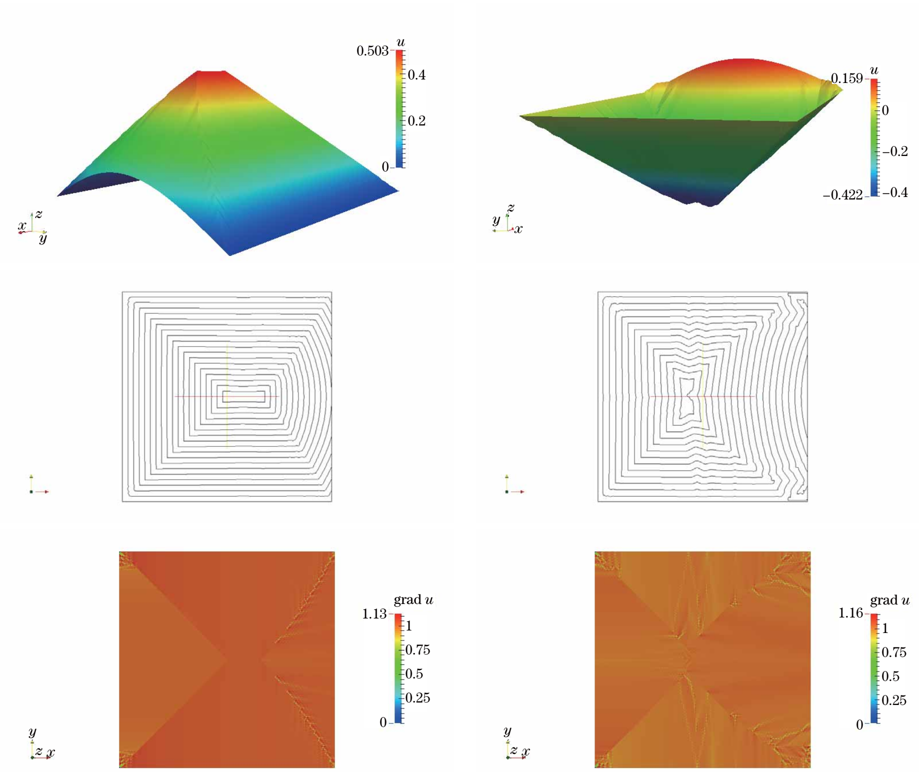

Figure 15 Non-homogeneous boundary conditions on the unit square (III). Approximation u_h of the solution of the Eikonal equation $\left(h = \frac{1}{150}\right.$, after 500 iterations$\left.\right)$. First row: Graph of u_h; second row: Contours of $|u_h|$; third row: Visualization of $|\nabla u_h|$. Left: Maximal solution; right: Minimal solution.

and affine functions. The imposition of these boundary conditions do not jeopardize the global convergence properties of the algorithm.

7.6 A CFD application

Finally, let us qualitatively describe the use of the Eikonal equation for an application in computational fluid dynamics. When modeling turbulence in computational fluid dynamics, several models involve a mixing length (see [39]). Namely, the local turbulent viscosity is a function of the distance between the given point and the boundary of the computational domain. The proposed algorithm can be used to easily compute the distance to the boundary for any arbitrary domain Ω.

As an illustration, let us consider a two dimensional cut of an aluminum Hall-Héroult cell (see, e.g., [23] for details). Dimensions are approximately 3 [m] $\times$ 0.4 [m]. In applications, a magneto-hydrodynamic problem has to be solved in such a domain; the computation of velocity and pressure fields via the solution of the Navier-Stokes equations usually involves turbulence effects.

Figure 16 visualizes the approximation of the distance obtained with our algorithm for this

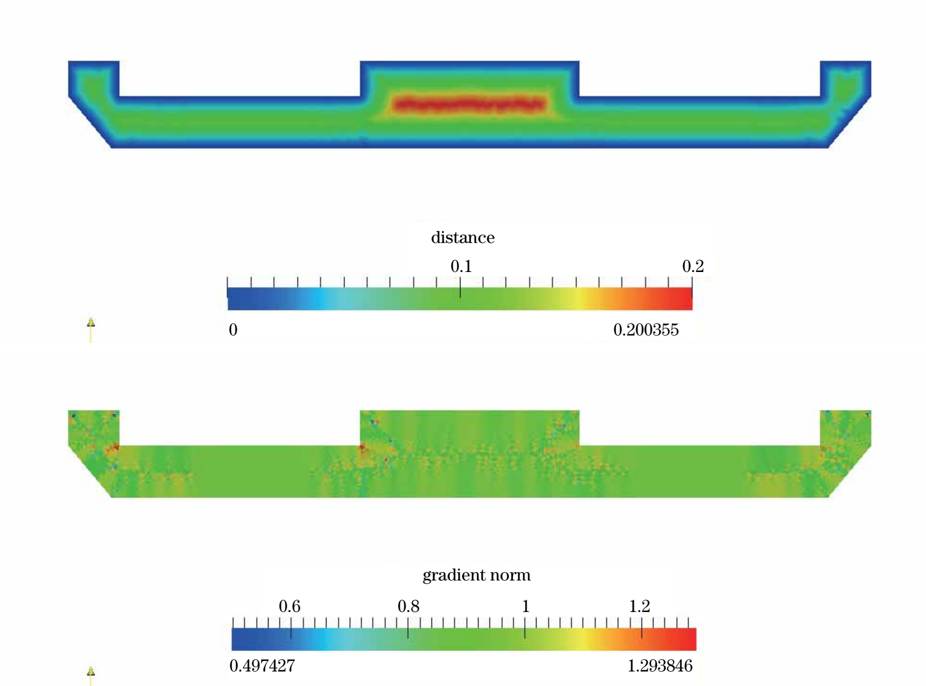

Figure 16 CFD application. Distance to the boundary for industrial application. Top: Contours of the approximation u_h of the solution of the Eikonal equation. Bottom: Piecewise constant approximation $|\nabla u_h|$.

particular geometry. The boundary data is $g(x_1, x_2) = 0$ for all $(x_1, x_2) \in \partial\Omega$, so that the solution is the distance to the boundary. The mesh contains approx. 3300 nodes and 6600 elements. Typical CPU time is around 20 [s] per outer iteration and a satisfactory stationary solution can be obtained after approx. 10 iterations. The gradient norm is equal to one almost everywhere, except in the corners of the domain (especially the entrant corners where the domain is not convex).

8 Viscosity Solution Interpretation

Let us briefly describe the viscosity solution interpretation of the approximated solutions obtained with this penalty-regularization-operator splitting method. Despite the fact that the proposed algorithm is variational in nature, and relies on elliptic solvers, one can write it as the solution to some viscosity equation.

Let us suppose that Ω is simply connected, and define $\mathbf{v} = \{v_1, v_2\}$ by $v_1 = \frac{\partial u}{\partial x_2}$ and $v_2 = -\frac{\partial u}{\partial x_1}$, and $\mathbf{v}_1$ by $\mathbf{v}_1 = \left\{\frac{\partial u_1}{\partial x_2}, -\frac{\partial u_1}{\partial x_1}\right\}$. We can easily show that (4.8) can be rewritten as

$$\begin{cases} -\eta\nabla^2\mathbf{v} + \mathbf{v} + \varepsilon_2^{-1}(|\mathbf{v}|^2 - 1)\mathbf{v} + \nabla p = C\mathbf{v}_1 & \text{in } \Omega, \\ \nabla \cdot \mathbf{v} = 0 & \text{in } \Omega, \end{cases} \tag{8.1}$$

together with appropriate boundary conditions. Problem (8.1) is a kind of Ginzburg-Landau nonlinear Stokes problem. It emphasizes that u is linked to the solution $\mathbf{v}$ of a (kind of) viscous fluid flow equation.

9 Concluding Remarks and Perspectives

A numerical method for the approximation of the Dirichlet problem for the Eikonal equation $|\nabla u| = 1$ for arbitrary domains in two dimensions has been presented.

We have introduced an iterative algorithm based on the following ingredients: a penalization of the non-smooth constraint on the gradient, a linear or nonlinear, biharmonic regularization of the variational problem, and an operator-splitting approach to find a stationary solution of the corresponding dynamical flow problem.

Low-order finite elements have been used for the discretization, as the low regularity of the solution does not require any high-order approximations. Numerical results have shown the ability of our method in approximating solutions of the Eikonal equation for various two-dimensional domains and various boundary data. In particular, our methodology can handle quite easily and accurately (convex) domains with curved boundaries. Cases with exact known solutions have allowed us to highlight the actual convergence properties of our methodology.

Further work will include the extension of this Eikonal equation to the vectorial case, namely, to find $\mathbf{u} : \mathbb{R}^2 \to \mathbb{R}^2$ satisfying

$$\begin{cases} \nabla \mathbf{u} \in \mathcal{O}(2) & \text{in } \Omega, \\ \mathbf{u} = \mathbf{g} & \text{on } \partial\Omega, \end{cases}$$

where $\mathcal{O}(2)$ denotes the set of the 2×2 orthogonal matrices. This problem arises in the origami theory (see for instance [15–17]). The authors believe that the approach proposed in this article will apply naturally to this vectorial extension.

Acknowledgments The authors would like to thank Prof. Dacorogna B. (EPFL) for fruitful discussions and suggesting the investigation of such non-smooth problems. The first author thanks Prof. Picasso M. and MATHICSE (EPFL) for partial financial support.

References

[1] Aronsson, G., Evans, L. C. and Wu, Y., Fast/slow diffusion and growing sandpiles, *Journal of Differential Equations*, **131**, 1996, 304–335.

[2] Barth, T. J. and Sethian, J. A., Numerical schemes for the Hamilton-Jacobi and level set equations on triangulated domains, *J. Comput. Phys.*, **145**(1), 1998, 1–40.

[3] Caboussat, A. and Glowinski, R., A numerical method for a non-smooth advection-diffusion problem arising in sand mechanics, *Commun. Pure Appl. Anal*, **8**(1), 2008, 161–178.

[4] Caboussat, A. and Glowinski, R., Regularization methods for the divergence equation $\nabla \cdot \mathbf{u} = f$, *J. Comput. Math.*, **30**(4), 2012, 354–380.

[5] Caboussat, A., Glowinski, R. and Pan, T. W., On the numerical solution of some Eikonal equations: An elliptic solver approach, to appear of Contemporary Applied Mathematics, Higher Education Press, Beijing and World Scientific, Singapore, 2013.

[6] Caboussat, A., Glowinski, R. and Sorensen., D. C., A least-squares method for the numerical solution of the Dirichlet problem for the elliptic Monge-Ampère equation in dimension two, *ESIAM: Control, Optimization and Calculus of Variations*, **19**(3), 2013, 780–810.

[7] Caffarelli, L. and Crandall, M. G., Distance functions and almost global solutions of Eikonal equations, *Comm. Partial Differential Equations*, **3**, 2010, 391–414.

[8] Caffarelli, L. A. and Cabré, X., Fully Nonlinear Elliptic Equations, American Mathematical Society Colloquium Publications, **43**, Providence, RI, 1995.

[9] Caffarelli, L. A. and Glowinski, R., Numerical solution of the Dirichlet problem for a Pucci equation in dimension two. Application to homogenization, *J. Numer. Math.*, **16**(3), 2008, 185–216.

[10] Chan, T. and Shen, J., Image Processing and Analysis: Variational, PDE, Wavelet, and Stochastic Methods, SIAM, Philadelphia, 2005.

[11] Crandall, M., Evans, L. and Lions, P. L., Some properties of viscosity solutions of Hamilton-Jacobi equations, *Trans. Amer. Math. Soc.*, **282**, 1984, 487–502.

[12] Dacorogna, B., Glowinski, R., Kuznetzov, Y. and Pan, T. W., On a conjuguate gradient/Newton/penalty method for the solution of obstacle problems. application to the solution of an Eikonal system with Dirichlet boundary conditions, Křížek, M., Neittaanmäki, P., Glowinski, R. and Korotov, S., editors, Conjugate Gradient Algorithms and Finite Element Methods, Springer-Verlag, Berlin, Heidelberg, 2004, 263–283.

[13] Dacorogna, B., Glowinski, R. and Pan, T. W., Numerical methods for the solution of a system of Eikonal equations with Dirichlet boundary conditions, *C. R. Acad. Sci. Paris, Sér. I*, **336**, 2003, 511–518.

[14] Dacorogna, B. and Marcellini, P., Implicit Partial Differential Equations, Birkhaüser, Basel, 1999.

[15] Dacorogna, B., Marcellini, P. and Paolini, E., An explicit solution to a system of implicit differential equations, *Ann. Inst. Henri Poincaré, Analyse Non Linéaire*, **25**, 2008, 163–171.

[16] Dacorogna, B., Marcellini, P. and Paolini, E., Lipschitz-continuous local isometric immersions: Rigid maps and origami, *Journal Math. Pures Appl.*, **90**, 2008, 66–81.

[17] Dacorogna, B., Marcellini, P. and Paolini, E., Origami and partial differential equations, *Notices of the American Math. Soc.*, **57**, 2010, 598–606.

[18] Dean, E. J. and Glowinski, R., Numerical methods for fully nonlinear elliptic equations of the Monge-Ampère type, *Comp. Meth. Appl. Mech. Engrg.*, **195**, 2006, 1344–1386.

[19] Dean, E. J. and Glowinski, R., On the numerical solution of the elliptic Monge-Ampère equation in dimension two: A least-squares approach, in Glowinski, R. and Neittaanmäki, P., editors, Partial Differential Equations: Modeling and Numerical Simulation, **16**, Computational Methods in Applied Sciences, Springer-Verlag, 2008, 43–63.

[20] Dean, E. J., Glowinski, R. and Guidoboni, G., On the numerical simulation of Bingham visco-plastic flow: Old and new results, *Journal of Non Newtonian Fluid Mechanics*, 142, 2007, 36–62.

[21] Delbos, F., Gilbert, J. C., Glowinski, R. and Sinoquet, D., Constrained optimization in seismic reflection tomography: A Gauss-Newton augmented Lagrangian approach, *Geophysical Journal International*, **164**, 2006, 670–684.

[22] Evans, L. C., Partial Differential Equations, **19**, Graduate Texts in Mathematics, American Mathematical Society, 1998.

[23] Flück, M., Hofer, T., Picasso, M., et al., Scientific computing for aluminum production, *Int. J. Numer. Anal. and Modeling*, **6**(3), 2009, 489–504.

[24] Glowinski, R., Finite Element Method for Incompressible Viscous Flow, **IX**, Handbook of Numerical Analysis (Ciarlet, P. G., Lions, J. L., eds), Elsevier, Amsterdam, 2003, 3–1176.

[25] Glowinski, R., Numerical Methods for Nonlinear Variational Problems, Springer-Verlag, New York, NY, 2nd edition, 2008.

[26] Glowinski, R., Numerical methods for fully nonlinear elliptic equations, Invited Lectures, 6th Int. Congress on Industrial and Applied Mathematics, EMS, Zürich, Switzerland, 2009, 155–192.

[27] Glowinski, R., Kuznetzov, Y. and Pan, T. W., A penalty/Newton/conjugate gradient method for the solution of obstacle problems, *C. R. Acad. Sci. Paris, Sér. I*, **336**, 2003, 435–440.

[28] Glowinski, R., Lions, J. L. and Trémolières, R., Numerical Analysis of Variational Inequalities, Studies in Mathematics and Its Applications, North-Holland Publishing Co., Amsterdam, New York, 1981.

[29] Gremaud, P. A. and Ide, N. R., Computation of nonclassical solutions to Hamilton-Jacobi problems, *SIAM J. Sci. Comput.*, **21**, 1999, 502–521.

[30] Gremaud, P. A. and Kuster, C. M., Computational study of fast methods for the Eikonal equation, *SIAM J. Sci. Comp.*, **27**, 2006, 1803–1816.

[31] Hysing, S. R. and Turek, S., The Eikonal equation: Numerical efficiency vs algorithmic complexity on quadrilateral grids, Proceedings of Algorithmy, 2005, 22–31.

[32] Kimmel, R. and Sethian, J. A., Computing geodesic paths on manifolds, *Proceedings of National Academy of Sciences*, **95**(15), 1998, 8431–8435.

[33] Majava, K., Glowinski, R. and Kärkkäinen, T., Solving a non-smooth eigenvalue problem using operator-splitting methods, *International Journal of Computer Mathematics*, **84**(6), 2007, 825–846.

[34] Nečas, J., Introduction to the Theory of Nonlinear Elliptic Equations, John Wiley & Sons, Ltd., Chichester, 1986.

[35] Prigozhin, L., Sandpiles and rivers networks: Extended systems with nonlocal interactions, *Phys. Rev. E*, **49**(2), 1994, 1161–1167.

[36] Prigozhin, L., Variational model of sandpile growth, *Euro. Journal of Applied Mathematics*, **7**, 1996, 225–235.

[37] Qin, F., Luo, Y., Olsen, K., et al., Finite-difference solution of the Eikonal equation along expanding wavefronts, *Geophysics*, **57**(3), 1992, 478–487.

[38] Rockafellar, R. T., Convex Analysis, Princeton University Press, Princeton, NJ, 1997.

[39] Schlichting, H. and Gersten, K., Boundary Layer Theory, McGraw and Hill, 8th revised edition, Springer-Verlag, Berlin, 2000.

[40] Sethian, J. A., Fast marching methods, *SIAM Rev.*, **41**(2), 1999, 199–235.

[41] Sethian, J. A. and Vladimirsky, A., Fast methods for the Eikonal and related Hamilton-Jacobi equations on unstructured meshes, *Proceedings of National Academy of Sciences*, **11**, 2000, 5699–5703.

[42] Zhao, H., A fast sweeping method for Eikonal equations, *Math. Comp.*, **74**, 2005, 603–627.